Glaciers and Nutrients in the Canadian Arctic Archipelago Marine System

Maya P. Bhatia[1]*, Stephanie Waterman[2], David O. Burgess[3], Patrick L. Williams[1], Randelle M. Bundy[4], Travis Mellett[4], Megan Roberts[5], and Erin M. Bertrand[5]*

[1] Department of Earth and Atmospheric Sciences, University of Alberta, Edmonton, AB, Canada

[2] Department of Earth, Ocean & Atmospheric Sciences, University of British Columbia, Vancouver, BC, Canada

[3] Geological Survey of Canada, Natural Resources Canada, Ottawa, ON, Canada

[4] School of Oceanography, University of Washington, Seattle, WA, USA

[5] Department of Biology, Dalhousie University, Halifax, NS, Canada

* co-corresponding

Key Points

Marine waters fed by tidewater glaciers in the Canadian Arctic have elevated macro- and micro-nutrient concentrations

Upwelling of deeper marine waters drives macronutrient enrichments, while micronutrient enrichments are driven directly by glacial discharge

As Canadian Arctic glaciers melt, local and regional marine productivity may be impacted by changes in nutrient delivery

Abstract

The Canadian Arctic Archipelago (CAA) is vulnerable to climate warming, and with over 300 tidewater glaciers, is a hotspot for enhanced glacial retreat and meltwater runoff to the ocean. In contrast to Greenlandic and Antarctic systems, CAA glaciers and their impact on the marine environment remain largely unexplored. Here we investigate how CAA glaciers impact nutrient delivery to surface waters. We compare water column properties in the nearshore coastal zone along a continuum of locations, spanning those with glaciers (glacierized) to those without (non-glacierized), in Jones Sound, eastern CAA. We find that surface waters of glacierized regions contain significantly more macronutrients (nitrogen, silica, phosphorus) and micronutrients (iron, manganese) than their non-glacierized counterparts. Water column structure and chemical composition suggest that macronutrient enrichments are a result of upwelling induced by rising submarine discharge plumes, while micronutrient enrichments are driven directly by glacial discharge. Generally, the strength of upwelling and associated macronutrient delivery scales with tidewater discharge volume. Glacier-driven delivery of the limiting macronutrient, nitrate, is of particular importance for local productivity, while metal delivery may have consequences for regional micronutrient cycling given Jones Sound's important role in modifying water masses flowing into the North Atlantic. Finally, we use the natural variability in glacier characteristics observed in Jones Sound to consider how nutrient delivery may be affected as glaciers retreat. The impacts of melting glaciers on marine ecosystems through both these mechanisms will likely be amplified with increased meltwater fluxes in the short-term, but eventually muted as CAA ice masses diminish.

Plain Language Summary

The Canadian Arctic Archipelago (CAA) contains many glaciers that are vulnerable to global warming. Many of these glaciers terminate in the ocean, meaning that as they melt, they deliver materials directly into the coastal ocean, often below the sea surface. This glacier meltwater can deliver nutrients that may enhance marine productivity, but this has not yet been systematically examined in the CAA. Here we compare concentrations of essential macronutrients (nitrogen, silica, phosphorus), and micronutrients (iron, manganese) in areas with glaciers and without, in the Jones Sound region of the CAA. We find elevated concentrations of nutrients in marine waters surrounding areas with glaciers. The source of macronutrients are deeper marine waters that are carried to the surface by rising glacier meltwater entering the ocean below the sea surface, while the source of micronutrients is glacier meltwater itself. Much of the water that flows from the Arctic Ocean into the North Atlantic does so through CAA passageways that receive this glacier input. Understanding how glacier-driven nutrient delivery is likely to change as the climate continues to warm will help us predict changes in marine productivity both locally in the CAA and in regions of the North Atlantic that receive CAA water.

1 Introduction

Delivery of meltwater and materials from glaciers to the ocean is accelerating due to climate warming, with important and poorly-characterized consequences for the marine environment. While the contributions of these shrinking ice masses to sea level rise are undisputed, their role in marine biogeochemical processes is just beginning to be revealed. Recent studies have shown that glacial meltwater discharge can affect nutrient supply (Bhatia et al., 2013; Hawkings et al., 2015; Kanna et al., 2018), carbon export (Hawkings et al., 2017; Wadham et al., 2019), carbonate chemistry (Cantoni et al., 2020; Fransson et al., 2015; Meire et al., 2015), fjord-scale estuarine circulation (Lydersen et al., 2014; Straneo & Cenedese, 2015), and patterns of primary productivity (Etherington et al., 2007; Hopwood et al., 2019; Juul-Pedersen et al., 2015). Climate warming has significantly increased glacial melt and runoff (Bliss et al., 2014; King et al., 2020), and glacial fluxes are predicted to increase further before ultimately disappearing. The Canadian Arctic Archipelago (CAA) is a key hotspot for such changes (Cook et al., 2019; Gardner et al., 2011), and after Greenland and Antarctica, is one of the largest contributors of glacier meltwater to the global ocean (Box et al., 2018). Roughly two thirds of the water flowing from the Arctic Ocean into the North Atlantic is routed through the CAA (Zhang et al., 2016). Yet, we know little about the effects of shrinking glaciers in the CAA on regional and coastal hydrography and biogeochemistry, and even less about their role in influencing the biogeochemistry of Arctic waters as they make their way into the North Atlantic.

Elevated marine productivity associated with glaciers has been noted as early as 1938 around Greenland (Greisman, 1979; Hartley & Dunbar, 1938), and in 1973 in the most recent study on this topic in the CAA (Apollonio, 1973). Contemporary work in Alaska (Etherington et al., 2007; Hood & Scott, 2008), Svalbard (Halbach et al., 2019; Lydersen et al., 2014), and Greenland (Hopwood et al., 2018; Meire et al., 2017) have highlighted the significant role that glaciers might play in elevating key nutrient (e.g. nitrate, phosphate, silicate, iron) concentrations in surface waters within fjords (Hawkings et al., 2016; Kanna et al., 2020; Kanna et al., 2018) and beyond to the surrounding continental shelf (Cape et al., 2018). This glacial stimulation of nutrient delivery may be particularly significant because it occurs during a critical period when surface plankton are nutrient-limited after the spring bloom but when insolation is still plentiful (Arrigo et al., 2017). Since nitrate is often the limiting nutrient in coastal Arctic summer surface

105 waters (Randelhoff et al., 2020), it has been the particular focus of recent investigations (Beaton
106 et al., 2017; Kanna et al., 2018; Meire et al., 2017). In glacial fjords, a likely source of this
107 growth-limiting resource can be deep seawater entrained into the photic zone by low-density
108 meltwaters that rise rapidly through the water column near the glacier terminus (Hopwood et al.,
109 2018; Kanna et al., 2018; Meire et al., 2017). This mechanism of nitrogen delivery to surface
110 waters can however only be present downstream from tidewater glaciers where the meltwater
111 discharge exits the ice front well below the surface (Hopwood et al., 2018). In contrast,
112 meltwater runoff from land-terminating glaciers which discharges to marine waters at the
113 surface, forms a surface freshwater cap, stratifying the water column and impeding vertical
114 transport of nutrient-rich deeper waters (Hopwood et al., 2019). Previous studies in Greenland
115 comparing fjords with tidewater and land-terminating glaciers have observed markedly
116 decreased productivity in the latter (Holding et al., 2019; Meire et al., 2017). In tidewater glacial
117 fjords, primary productivity is often enhanced distal to the glacier front when the majority of the
118 discharge sediment has settled out and turbidity decreases (Juul-Pedersen et al., 2015; Kanna et
119 al., 2018; Meire et al., 2017). The enhanced primary productivity in association with tidewater
120 glaciers has been tied to greater fixed carbon export to the deep ocean via a stronger biological
121 pump (Hawkings et al., 2018b; Seifert et al., 2019). Finally, this positive effect on primary
122 production appears to extend up the food chain, as tidewater glaciers in Greenlandic fjords have
123 been associated with locally-enhanced harvest of higher trophic levels (e.g., fish, seals) (Everett
124 et al., 2018; Meire et al., 2017). Pre-dating formal scientific studies is traditional knowledge
125 from Inuit communities which indicates that waters off the termini of tidewater glaciers are rich
126 in wildlife (J. Qaapik, Grise Fiord Rangers). In addition, seabirds have long been known to
127 congregate at the calving front, foraging on zooplankton brought to the surface by the rising
128 subglacial freshwater plume (Lydersen et al., 2014).

129 Glaciers can also play an important role in metal micronutrient delivery and cycling. In
130 particular, glacial meltwater has been shown to be enriched in iron (Fe) and some other metal
131 micronutrients like manganese (Mn) as a result of weathering processes, suggesting that this
132 meltwater may serve as a direct source of metals to the ocean (Bhatia et al., 2013; Hawkings et
133 al., 2014). However, many unknowns remain about how much of the metals delivered by glaciers
134 is ultimately bioavailable in the ocean (Hopwood et al., 2019; Wadham et al., 2019). Factors
135 influencing this include the degree of estuarine removal (Boyle et al., 1977), the mineralogy of

the glacial system (Hawkings et al., 2018a; Raiswell et al., 2018), and organic carbon interactions (Zhang et al., 2015), each of which are expected to vary considerably between glacier systems. Estimates of the spatial scales over which glaciers can influence marine metal availability in the ocean are variable and uncertain, but range from 10s to 100s of kilometers (Hopwood et al., 2019), suggesting that both local and regional metal cycling may be influenced by glaciers. Marine systems off Greenland and Antarctica can be micronutrient limited (Hawkings et al., 2014; Krisch et al., 2020), and so constraining micronutrient delivery from glacier meltwater can be important for determining the impact of glaciers on local productivity in those systems. While metal micronutrients are not expected to limit productivity in the CAA, they can be present in extremely low concentrations in Baffin Bay and regions of the North Atlantic (Colombo et al., 2020) that are fed by waters modified in the CAA (Zhang et al., 2016). As such, the role of CAA glaciers in metal micronutrient delivery and cycling has the potential to impact regional phytoplankton growth and carbon cycling.

Much of our current understanding about the impact of glaciers on marine biogeochemistry and productivity is based on studies conducted in Greenland, yet, glaciers in the CAA are distinct in important ways. One difference of particular significance to nutrient delivery is that of the grounding line depth typical of the CAA. The CAA is dominated by smaller, shallower marine-terminating glaciers. In the northern CAA (Queen Elizabeth Islands) grounding lines are on average ~230-m depth, shoaling even more in the southern CAA (Baffin and Bylot Islands) to an average of ~100-m depth (Van Wychen et al., 2014; Van Wychen et al., 2015). Indeed, only eight glaciers across the whole region have grounding lines greater than 300-m depth (Van Wychen et al., 2015). By comparison, many outlet glaciers draining the Greenland Ice Sheet terminate into fjords at depths of 600 m or more (Carroll et al., 2016). Previous studies of Greenlandic glacier systems have identified grounding line depth as a primary control on the degree to which the plume-driven entrainment delivers macronutrient-enriched deep seawater to the photic zone (Hopwood et al., 2018; Oliver et al., 2020). Using a subglacial discharge plume model for an idealized Greenlandic-like marine-terminating glacier, Hopwood et al. (2018) estimate that the optimum grounding line depth for nitrate upwelling into the photic zone occurs at 580-m depth. These model results show that a key control on nitrate supply to the photic zone is the relationship between the meltwater discharge depth and the nutricline depth: at shallower glaciers where submarine discharge shoals, meltwater plumes are no longer expected to entrain

seawater below the nutricline and nitrate supply to the photic zone is expected to be diminished. However, there are limited observations at glaciers with grounding lines less than 250-m depth; as such the impacts of shallow tidewater glaciers with respect to nutrient delivery remain largely unknown. Today, coastal areas with many glaciers, like West Antarctica, Greenland, Svalbard, the Gulf of Alaska and the CAA, disproportionately experience the impacts of glacial meltwater on their marine ecosystems and, in the future, the inevitable changes that will ensue as tidewater glaciers retreat due to climate warming. Understanding how these impacts vary with differing meltwater fluxes and depths of tidewater glacier input is important for accurate future projections of high-latitude marine ecosystem productivity and nutrient cycling as the climate changes.

In this study we investigate how tidewater glacier input impacts water column properties and nutrient delivery to the euphotic zone at six sites in the CAA which represent a spectrum of glacier forcing with respect to depth and volume of meltwater discharge. Our study builds directly on the most recent investigation exploring the impact of glaciers on nutrients in the marine environment in the CAA, conducted half a century ago in Jones Sound, NU Canada (Apollonio, 1973). Jones Sound is home to the Inuit hamlet of Ausuittuq (Grise Fiord) and is a marine region surrounded by glaciers draining large ice fields and caps on Ellesmere and Devon Islands. Traditional knowledge from hamlet community members indicates that the termini of tidewater glaciers in this region are rich in wildlife, providing hunting grounds for hamlet citizens. Here, we explore the nearshore coastal zone of a continuum of systems in this region. These sites span those which are presently occupied by relatively deep (> 200-m depth) marine-terminating glaciers with a large proportion of their calving front in the ocean, to sites with shallow (< 50-m depth) tidewater glaciers, and finally to sites with no glaciers present. As Arctic temperatures continue to rise, most tidewater glaciers in the CAA will experience accelerated melting, inevitably retreat from the ocean, and ultimately disappear (Cook et al., 2019). As a result, any glacially-mediated delivery of macro- and micro-nutrients to the marine environment will likely increase in the short term and then cease, thus fundamentally altering the hydrography and biogeochemistry of the CAA coastline. Results from this study further our understanding of glacier-ocean interactions in the CAA and beyond, providing baseline data critical for understanding the implications of melting glaciers on marine ecosystem productivity, function and health.

198

199 **2 Study Site**

200

201 ***2.1 Glacier Inputs***

202

203 Qikiqtaaluk (Jones Sound, Nunavut Canada) is a waterway situated between Devon and
204 Ellesmere Islands in the Canadian Arctic Archipelago (CAA) that is inundated each summer
205 with glacial meltwater draining the Devon Ice Cap on Devon Island to the north and the Sydkap
206 and Manson Ice Fields on Ellesmere Island to the south.

207 The 12,050 km^2 (3,980 km^3) Devon Ice Cap is one of the largest ice masses in the CAA.
208 It is comprised of a cold-based interior frozen to the bed, and is drained by fast-flowing warm-
209 based dynamic outlet glaciers (Burgess et al., 2005; Dowdeswell et al., 2004; Van Wychen et al.,
210 2017) most of which terminate at tidewater. The 42-km long Belcher Glacier drains the northeast
211 sector of the Devon Ice Cap, terminating in eastern Jones Sound into a region open to Smith
212 Sound and the head of Baffin Bay (Figure 1). Ice flow velocities in the heavily crevassed
213 terminus region of Belcher Glacier have been accelerating steadily over the past decade,
214 exceeding 600 m per year in 2020 (Wychen et al., 2021). Consequently, mass loss due to iceberg
215 calving from the Belcher Glacier accounts for >50% of the mass loss due to calving from all
216 tidewater glaciers on Devon Ice Cap. Sea-floor mapping surveys reveal water depths of ~200 m
217 near the terminus until a sharp break in slope ~2 km from the ice front, beyond which depths
218 eventually reach > 600 m in the open ocean, ~10 km from the Belcher Glacier terminus
219 (Batchelor et al., 2016). To the west of Belcher Glacier, the 26-km long Sverdrup Glacier drains
220 northward from Devon Ice Cap to enter Brae Bay in the south-central region of Jones Sound.
221 Previous studies have shown that the Sverdrup and Belcher Glaciers both respond dynamically to
222 summer meltwater which acts to enhance flow by reducing friction along the glacier margins and
223 bed (Cress & Wyness, 1961; Danielson & Sharp, 2017). However, with a calving front less than
224 60 m thick and a flow of only ~40 m per year, Sverdrup Glacier is not a significant source of
225 iceberg discharge in comparison to Belcher Glacier. The bathymetry seaward from Sverdrup
226 Glacier is relatively unknown apart from limited observations of shallow water depths (< 10 m)
227 up to 10 km from the glacier terminus as indicated in marine charts (Canadian Hydrographic

Services Chart V-7310-CA273424) and exposed rock outcrops ~8 km offshore visible in LandSat imagery.

In comparison to the well-studied Devon Ice Cap (Boon et al., 2010), markedly little is known about both the Sydkap and Manson Ice Fields on nearby Ellesmere Island. The 31-km long Sydkap Glacier is located at the head of South Cape Fiord, which is also occupied by several smaller tidewater glaciers. South Cape Fiord is ~25 km long, terminating in western Jones Sound (Figure 1). Similar to Belcher Glacier, the Sydkap Glacier terminus has been accelerating steadily over the past decade and is currently flowing at ~200 m per year (Wychen et al., 2021). Approximately 120 km to the east, the 36-km long Jakeman Glacier, which drains the Manson Ice Field, terminates into the northeast sector of Jones Sound, but is less exposed to Baffin Bay compared to the terminus of Belcher Glacier. Similar to Sverdup and Belcher Glaciers (Dowdeswell et al., 2004), the termini of both Sydkap and Jakeman Glaciers are grounded with no evidence of floating tongues (Copland et al., 2003).

As described below, we examine the influence of these glaciers on the marine system through comparisons with nearby non-glacierized sites situated within similar geologic settings. The two non-glacierized sites we examine are Truelove and Grise Fiord (Figure 1). The Truelove site is located in a non-glacierized lowland region of Devon Island, ~30 km from Truelove Inlet. It receives freshwater input from the Truelove and Gully Rivers. By comparison, Grise Fiord is a long, narrow fjord extending ~38 km inland, with no glaciers reaching its shore. Geologically, the glacierized sites of Sydkap and Jakeman Glaciers and the non-glacierized site of Grise Fiord are all surrounded by Cambrian, Ordovician, and Silurian dolomites, limestones, sandstones and gypsum (Harrison et al., 2015). The non-glacierized site near the Truelove lowlands, as well as the glacierized sites of the Sverdrup and Belcher Glaciers, are all underlain by Canadian Shield granite, gneiss, and quartzite (Harrison et al., 2015).

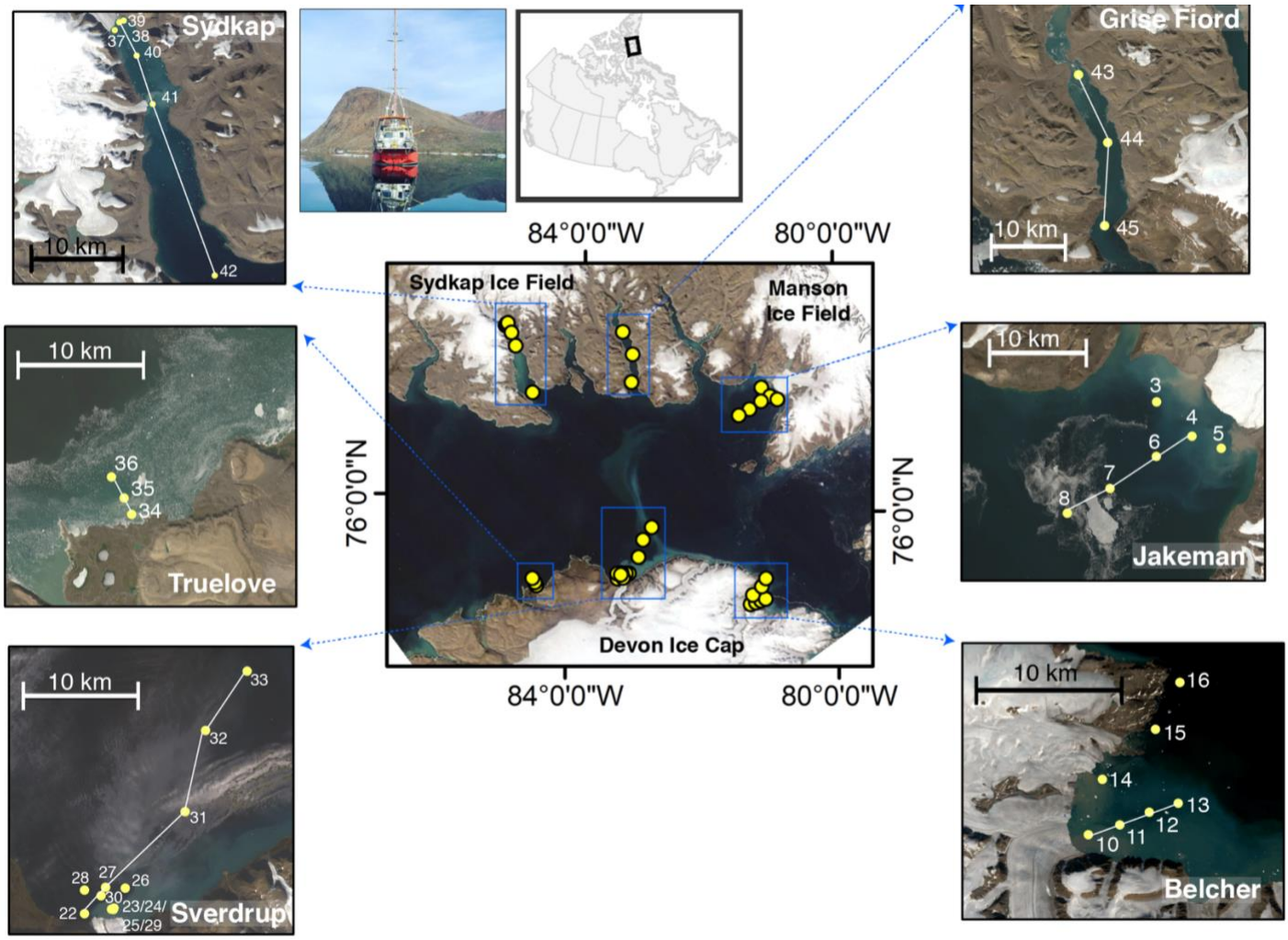

Figure 1. Map of study area in Qikiqtaaluk (Jones Sound, Nunavut) in the Canadian Arctic Archipelago using a MODIS image of the region from August 15, 2019. Blue boxes highlight six primary study sites, consisting of four tidewater glacier sites (Belcher, Sydkap, Sverdrup, and Jakeman Glaciers) and two sites without glaciers (Truelove and Grise Fiord). Insets to the left and right show enlarged views of the study sites using Landsat imagery from July and August 2019. Marine sampling stations are indicated by yellow symbols. Transects out from the glacier terminus / non-glacierized coast are indicated by the white lines. Insets above show the *S/Y Vagabond* from which shipboard operations were conducted and the location of the study area (black box).

2.2 Oceanographic Setting

The CAA is a transitional region where nutrient-rich Pacific waters that enter the Arctic Ocean via the Bering Strait are modified en route to Baffin Bay (Michel et al., 2006). Within the various channels of the archipelago, mixing and water mass modification occur, but the nutrient signatures of the Pacific source waters and, in particular, the signature of high silicate

concentration, remain (Michel et al., 2006). Waters arrive into Jones Sound from the deep basins of Arctic Ocean via pathways through the archipelago to the west, specifically via Hell Gate and Cardigan Strait, two narrow channels with strong southerly currents (Melling et al., 2008; Zhang et al., 2016). Waters also arrive into Jones Sound from the east, from northern Baffin Bay and Nares Strait, via Glacier Strait (Barber & Huyer, 1977). Circulation within Jones Sound is generally counter-clockwise, flowing westward on the north side (Ellesmere Island) and eastward on the south side (Devon Island), with outflow via Lady Ann Strait to Baffin Bay and ultimately the North Atlantic Ocean via Davis Strait (Barber & Huyer, 1977; Melling et al., 2008; Zhang et al., 2016). Outflow from Jones Sound is estimated to be ~17% of the total CAA outflow to the North Atlantic (Zhang et al., 2016).

3 Methods

3.1 Glaciological Comparisons

To better understand the different glacier systems examined in this study, we characterized several key attributes central to determining glacial forcing of nutrient delivery to the ocean including: terminus width, recent terminus retreat, the rate of summer meltwater runoff, ice thickness at the terminus, and elevation of the glacier bed at the terminus. The datasets used for basin delineation and to infer glacier terminus width and retreat are shown in Table S1.

We manually digitized high resolution (15 m) panchromatic band Landsat-7 Enhanced Thematic Mapper and Landsat-8 Operational Land Imagery obtained from the United States Geological Survey (https://earthexplorerusgs.gov/) to infer terminus width (total and marine portions) as well as terminus retreat since 1999. We achieved maximum image contrast by using images acquired under snow-free/clear sky conditions. We corrected imagery for radiometric and geometric distortions (Burgess & Sharp, 2004; U.S.G.S., 2019), and projected to the UTM WGS84, Zone 17 coordinate system. We assumed that error in our measurements of glacier *terminus width*, derived from manually digitizing irregular line features in the LandSat images, was one percent of the total length measured (Keefer et al., 1991). Additional errors in measurements of glacier *terminus retreat* are due to the spatial co-registration between the 1999

and 2019/2020 individual images. Based on the maximum horizontal displacement measured between several prominent bedrock features common in both images, we found the maximum co-registration error for all image pairs to be +/- 100 m in a northwest–southeast orientation. Thus, we estimated the total error, calculated from the square root sum-of-squares for human and co-registration error, to be +/- 116 m.

Cumulative daily melt runoff during the summer of 2019 was modelled from the RACMO2.3 surface mass balance (SMB) model as described in (Williams et al., submitted). Uncertainties in the volume of meltwater fluxes were established through comparing the gridded RACMO2.3 SMB data with in-situ surface mass balance measurements from the Sverdrup Glacier basin as described in (Williams et al., submitted). Due to a lack of in situ measurements in the Sydkap, Jakeman, and Belcher basins, the uncertainties established for the Sverdrup basin were applied to all basins in this study as reported in Table 1.

Measurements of *ice thickness at the terminus* and *elevation of the glacier bed at the terminus* of the four glaciers examined in this study were collected in 2012 and 2014 as part of the NASA Operation Ice Bridge program (Paden, 2010, updated 2019). Ice thickness was measured from the Multi-coherent On-board Radar Depth sounder (McORDs) flown at a nominal height of 500 m above the ice surface; these measurements detected the ice-bed interface with an accuracy of +/-10 m (Gogineni et al., 2001). These data were tagged with precise GPS and laser altimetry ice surface height data to provide spatial accuracy of +/- 10 cm. While the flights attempted to follow the glacier centerlines, deviations from this path occurred by up to several hundreds of meters, primarily along non-linear sections of the target glaciers. The centreline transect data giving ice and bed elevation for each of the four glaciers are presented in Dataset S1. Here we used the elevation of the glacier bed at the terminus along this nominal centreline as an estimate for grounding line depth which we equated to depth of submarine discharge in the ocean.

3.2 Marine Sampling

We undertook marine field work in August 2019 aboard the polar *S/Y Vagabond* wherein we sampled four glacierized (i.e. proximate to Belcher, Sydkap, Sverdrup, and Jakeman Glaciers)

and two non-glacierized (i.e. at the Truelove, Grise Fiord sites) fjords/bays within Jones Sound (Figure 1). In total, we occupied 37 stations in Jones Sound across our six sites (Table S2). In the glacierized fjords/bays, we took samples as close to the glacier calving front as possible and then transected out to open sound water in an effort to track the meltwater plume progression (Figure 1). At Belcher Glacier, we sampled seven stations between 1 km and 7.2 km of the terminus; at Sydkap Glacier, six stations between 0.29 km and 30 km of the terminus; at Sverdrup Glacier, 12 stations between 0.70 km and 26 km of the terminus; and at Jakeman Glacier, six stations between 2.3 km and 19 km of the terminus. We similarly sampled the two non-glacierized sites (Truelove, Grise Fiord) similarly, beginning nearshore and transecting offshore (Figure 1). At Truelove, we sampled three stations between 0.65 km and 3.5 km of shore. At Grise Fiord, there is a constriction ~10 km from the head of the fjord, and we sampled three stations between 2 km and 15 km from this constriction point. The distance from shore/the glacier front where we began each transect was necessarily different due to differences in glacier hazards, bathymetry, and sea ice.

3.3 In situ Measurements

We collected in situ measurements of various water column properties using a RBR maestro^3 multi-channel logger (RBR Ltd, Ottawa) equipped with sensors for conductivity, temperature, pressure, dissolved oxygen, photosynthetic active radiation, chlorophyll *a* (Chl *a*), and turbidity. At each station, the logger was equilibrated at 5-m below the surface before being raised and lowered again via a hand-winch operated at a consistent speed of ~ 0.5 m/s. All data presented here was collected during the downcast. We processed the sensor measurements with the Ruskin software (https://rbr-global.com/products/software) and GSW Oceanographic Toolbox of TEOS-10 (McDougall & Barker, 2011), and averaged the data in 1-m depth bins. We present transect contour plots of all logger data in the Supplementary Material (Dataset S2).

3.4 Sample Collection and Analyses

We collected water column bottle samples using 10-L Model 1080 (non-metallic) GO-FLO sample bottles, with a Teflon coated messenger (General Oceanics, Miami). We dismantled and

cleaned the GO-FLO bottles prior to use, according to seawater trace-metal clean procedures (i.e. 0.1% Citranox soak, 3x MilliQ water rinse, isopropoal rinse, 12h 1.2M hydrochloric acid (HCl) soak, and 3 x MilliQ rinse, as described in Cutter and Bruland (2012)). We selected depths at which the bottles were triggered for sampling using the real-time logger profile to capture specific aspects of water column structure at each station. We generally collected samples at the surface, at the deep chlorophyll maximum (DCM) (if present), and at one or two deeper levels between 50 and 400 m depth. An exception is at Jakeman Glacier where the deepest bottle sample we could take was at 40 m depth due to challenging weather conditions.

We collected macronutrient (nitrate, NO_3^-; nitrite, NO_2^-; ammonia, NH_3^+; phosphate, PO_4^{3-}; and silicate, SiO_4) samples by directly filling a 60-mL syringe through silicon tubing from the GO-FLO bottle, and filtering through a 0.22 µm polyethersulfone (PES) syringe filter into clean (3.7% HCl soaked, MilliQ water rinsed), 3x sample-rinsed 20-mL HDPE plastic scintillation vials. We immediately froze nutrient samples upon collection, and these remained frozen until analysis. Nutrient concentrations were analyzed within 1 month of collection on a Skalar SAN++ Continuous Flow Nutrient Analyzer at the CERC.OCEAN Laboratory (McGrath et al., 2019). The limits of detections for NO_3^-, NO_2^-, NH_3^+, PO_4^{3-}, and SiO_4 concentrations were 0.3, 0.15, 0.01, 0.2, and 0.08 µM respectively.

Samples for total dissolvable metals were first collected from the GO-FLO bottle water on deck before any other water samples were acquired. Wearing trace metal grade gloves, we rinsed the GO-FLO spigot with dilute trace metal clean HCl and then 3x rinsed and filled trace metal clean 60 mL high density polyethylene (HDPE) bottles with unfiltered water, directly from the cleaned spigot. Metal samples were acidified with quartz distilled HCl (Thermo Fisher) to 0.024 M HCl (pH ~1.7–1.8) at the University of Washington and were left acidified for at least 6 months. Quantification of Fe and Mn concentrations was achieved by inductively coupled plasma mass spectrometry (ICP-MS). Acidified total dissolvable samples were syringe filtered through a 0.2 µm polycarbonate track etched (PCTE; check this) rinsed with 5% v/v Trace Metal Grade™ nitric acid (HNO_3; Thermo Fisher). The filtrate was then diluted by adding 125 µL to a final volume of 5 mL of 2% v/v quartz distilled nitric acid (Thermo Fisher). The dilutions were measured on an iCap ICP analyzer (Thermo Fisher) at the University of Washington and are reported here as total dissolvable Fe and Mn (TdFe, TdMn). Macronutrient and metal micronutrient concentrations for each sample is shown in Table S3.

We also collected water samples to analyze for Chl *a* concentration (Table S3) to validate the trends observed in the logger sensor data. We collected these samples from the GO-FLO bottle with silicon tubing into 3x sample-rinsed amber HDPC plastic bottles, and gently vacuum filtered through a 47-mm GF/F (Whatman) membrane in the dark. Generally, we filtered between 600-1600 mL of seawater for each Chl *a* sample. We wrapped the filter in foil and flash froze it in a liquid nitrogen charged dry shipper for transport, which remained frozen until analysis. We measured Chl *a* concentrations using a Turner Design AquaFluor Handheld Fluorometer following the EPA Method 445 (Arar & Collins 1997). We calibrated the fluorometer using a pure Chl *a* standard (C5753, Sigma). The limit of detection was 0.024 µg per liter seawater.

We performed all subsequent data analysis in the open-source programming language R using the *readr*, *tidyverse*, *dplyr*, *patchwork*, *forecast*, *ggplot2*, *esquisse viridis* and *LakeMetabolizer* packages. The numbers of samples and stations displayed in Figures 2-4 are summarized in Table S2.

4 Results

4.1 Glaciological comparisons

Table 1 summarizes key glaciological features of the four glacierized sites. Since 1999, the terminus positions of all four glaciers have retreated between 217 m and 1,928 m (+/- 100m). Other notable features are: (1) the summer meltwater discharge (not including the mass loss due to calving) from each glacier is a similar order of magnitude, with Belcher Glacier having the largest flux, followed by Jakeman, Svedrup, and Sydkap; (2) with the prominent exception of Jakeman Glacier (<25%), all glaciers have a large (>80%) proportion of their terminus cliff submerged in the ocean; (3) solid ice discharge through calving is approximately an order of magnitude greater from Belcher Glacier than all other glaciers in this study combined; (4) the submarine discharge at Sverdrup and Jakeman Glaciers is likely being released at a much shallower depth (<50 m depth) in comparison to that at the Belcher and Sydkap Glaciers (>200

m depth and >100 m depth, respectively). We expect that the submarine discharge is likely released at a greater depth than the bed elevation where the ice thickness was measured (listed in Table 1), since the meltwater streams likely erode deeper channels at the ice-bed interface where they exit the glacier (Catania et al., 2018). At Sverdrup Glacier in particular, we estimate the submarine discharge depth to be ≥ 30 m at the main discharge portal (Williams et al., submitted).

There are several physical factors that determine a tidewater glacier's potential influence on the recipient marine environment, such as the proportion of the ice terminus in the water, the depth of meltwater discharge into the ocean, and the meltwater discharge flux (Hopwood et al., 2019; Oliver et al., 2020; Wadham et al., 2019). Based solely on the proportion of the ice terminus in the water, we can broadly classify the marine environment distal to Belcher, Sydkap, and Sverdrup Glaciers as "strongly-tidewater-glacier-influenced" systems. We can classify Jakeman Glacier, comparatively, as a "weakly-tidewater-glacier-influenced" system, since 75% of its terminus is on land. By also considering the depth of submarine discharge and the meltwater flux, we can organize the four glaciers in this study along a continuum of stages in glacier retreat, with Belcher Glacier, the deepest tidewater glacier, and Jakeman Glacier, a glacier in recession to a land-terminating system, as the two extremes. Sydkap and Sverdrup Glaciers, with their intermediate grounding line depths (corresponding to the elevation of the glacier bed at the terminus listed in Table 1) and intermediate summer runoff fluxes, fall in between these extremes.

Table 1. Summary of characteristics of tidewater glaciers examined in this study. Bias-corrected melt runoff fluxes are reported for the 2019 summer melt season. Basin areas are from the Randolph Glacier Inventory v6 (RGI Constortium, 2017). Uncertainties for summer melt run-off flux, annual calving flux, elevation of the glacier bed at the terminus, and terminus retreat are indicated in brackets. Values in the last three columns (**ɤ**) were measured at the centerline only. The submarine discharge depth at Sverdrup Glacier (*) is likely deeper than indicated by the elevation of the glacier bed down the terminus centerline (details provided in text). Values for annual calving flux were obtained from Van Wychen et al. (2020). Ice thickness and elevation of glacier bed at the termini were obtained from NASA geophysical aerial surveys conducted in 2012 and 2014 (see Methods).

Glacier	**Location**	**Basin Area (km^2)**	**Glacier Terminus Width (km)**	**Width of Marine Terminating Portion (km)**	**Summer Melt Run-Off Flux (Gt/yr)**	**Annual Calving Flux (Gt/y)**	**Ice Thickness at Terminus (m)ɤ**	**Elevation of Glacier Bed at Terminus (m a.s.l.)ɤ**	**Terminus Retreat: 1999-2020 (m)ɤ**
Belcher	Devon Ice Cap, Devon Is.	1134	11.9	9.8	0.75 (0.14)	0.29 (0.031)	271	-239 (10)	1669 (100)
Sydkap	Sydkap Ice Field, Ellesmere Is.	491	3.09	3.09	0.13 (0.06)	0.042 (0.007)	190	-140 (10)	1928 (100)
Sverdrup	Devon Ice Cap, Devon Is.	805	5.12	5.12	0.34 (0.10)	0.006 (0.004)	25	-21* (10)	217 (100)
Jakeman	Manson Ice Field, Ellesmere Is.	670	12.9	3.1	0.55 (0.08)	N/A	51	-36 (10)	450 (100)

4.2 Comparisons of glacierized vs. non-glacierized marine sites

By comparing water properties in the near-surface ocean waters of glacierized (i.e. proximate to Belcher, Sydkap, Sverdrup, Jakeman Glaciers) and non-glacierized (i.e. at the Truelove, Grise Fiord sites) marine regions, we reveal stark contrasts in nutrient and turbidity distributions, but not Chl *a* concentrations (Figure 2). Mean, median, and maximum concentrations of all macronutrients (NO_3^-, PO_4^{3-}, SiO_4, and NH_3^+) as well as TdFe and TdMn in the upper 40 m of the water column (surface) were consistently higher at the glacierized compared to the non-glacierized sites (Table S4). Using a non-parametric Wilcoxon Rank Sum test to assess the significance of the differences, we show that nitrate, phosphate, silicate, iron, and manganese concentrations were all significantly ($p < 0.01$) higher in the samples from the glacierized sites. In contrast, ammonia concentrations were not significantly different between the glacierized and

non-glacerized sites ($p > 0.05$). Predictably, turbidity was significantly higher at the glacierized sites ($p < 0.0001$), consistent with the sources of particulate material being added to the marine system from the glaciers. As a result of these particle loads, the euphotic zone (calculated at 0.1% surface irradiance) was significantly deeper in the less turbid non-glacierized regions ($p < 0.0001$). Chl *a*, which may be influenced by both nutrient and light availability, was similar between the glacierized and non-glacierized regions ($p > 0.05$).

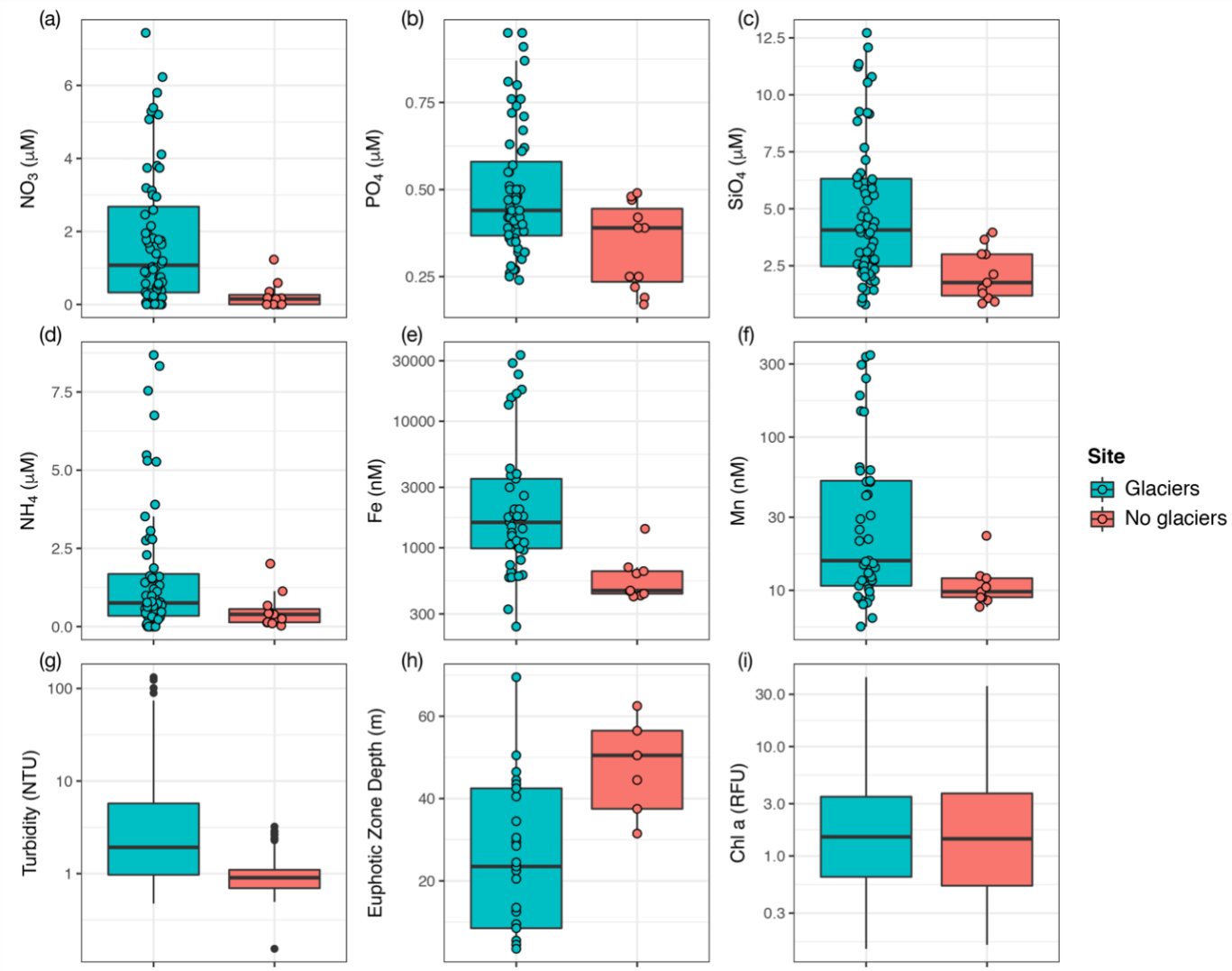

Figure 2. Comparisons of near-surface (upper 40 m) ocean water properties at glacierized (proximate to Belcher, Sydkap, Sverdrup, and Jakeman Glaciers) and non-glacierized (Truelove, Grise Fiord) sites. The individual bottle sample measurements are shown for macronutrient concentrations (a-d) (n = 60, glaciated and n = 11, unglaciated) and total dissolvable metal concentrations (e, f) (n = 41, glaciated, n = 9, unglaciated). Turbidity (g) and Chl *a* (i) data are from continuous sensor measurements through the water column. For euphotic zone depth (h), estimates (corresponding to 0.1% of surface PAR) at individual stations (n = 31, glaciated and n = 6, unglaciated) are shown. Note the log scale for Fe, Mn, turbidity and Chl *a*. The black bold horizontal line indicates the median value, and the lower and upper hinges correspond to the first (25th) and third (75th) quartiles, respectively. The whiskers extend to 1.5 times the interquartile range (distance between first and third quartile) in each direction, with outlier data beyond the whiskers plotted individually. Numbers of samples / stations are given in Table S2.

By comparing water properties as a function of distance from the glacier front/shore, we find systematic trends in surface nutrient concentrations and turbidity at glacierized sites (Figure 3), suggesting that differences between the glacierized and non-glacierized sites are linked to glacial activity. Specifically, we observed the highest median concentrations of NO_3^-, PO_4^{3-},

490 SiO_4, TdFe and TdMn in closest proximity to the glacier terminus. Comparatively, the non-
491 glacierized sites exhibited no systematic relationship for any nutrient with distance from shore.
492 Turbidity was also highest (median = 9.6 NTU) and the euphotic zone depth was the shallowest
493 (median = 8.5 m) at the stations closest to the ice front, with turbidity decreasing and euphotic
494 zone depth increasing with distance away from the terminus. In contrast, concentrations of Chl *a*,
495 which were more uniform between the glacierized and non-glacierized regions (Figure 2),
496 exhibited no systematic pattern in correlation with distance from the ice front, near-surface major
497 nutrient concentrations, or euphotic zone depth.

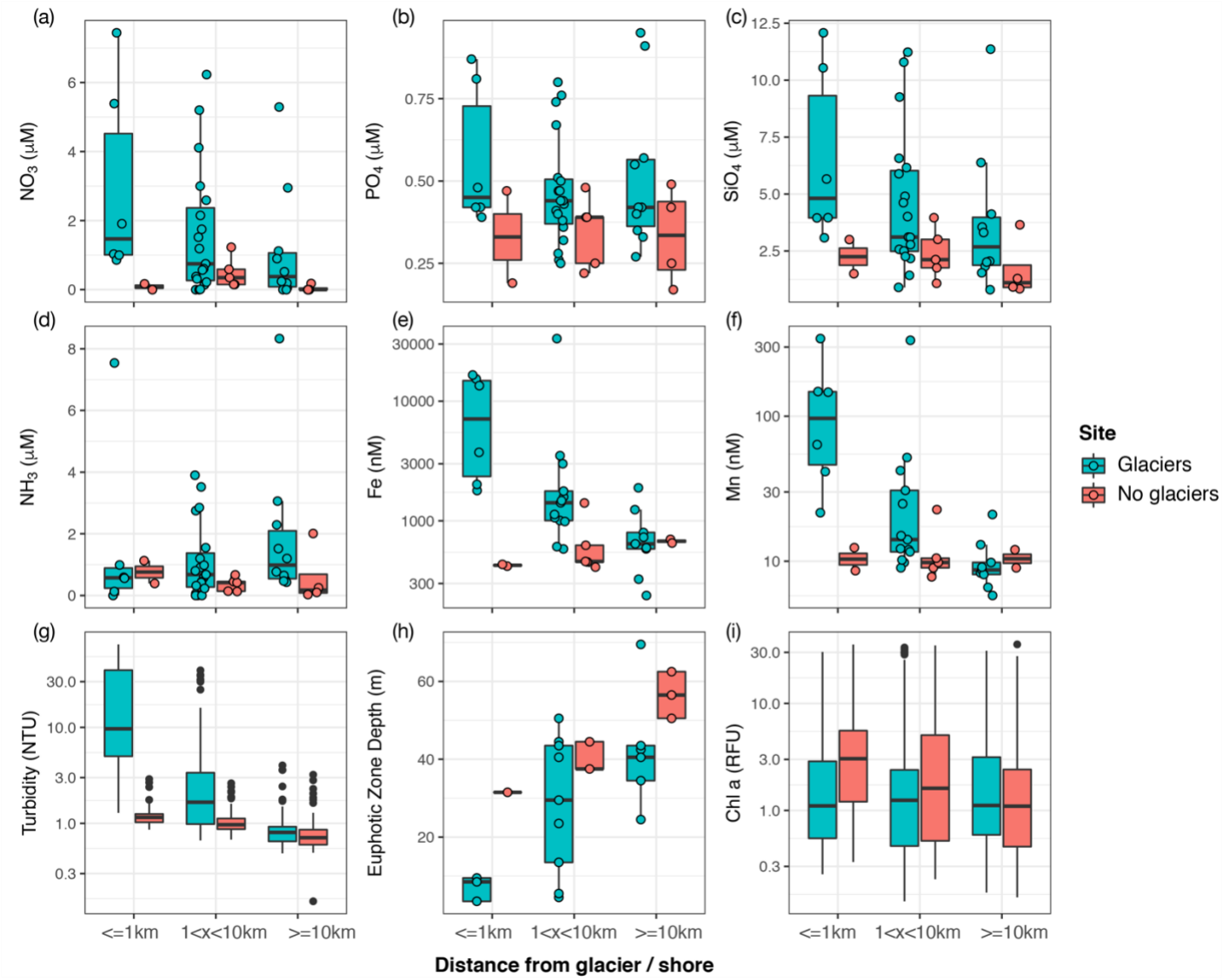

Figure 3. Comparisons of surface (upper 40 m) ocean water properties in glaciated (proximate to Belcher, Sydkap, Sverdrup, and Jakeman Glaciers) and non-glacierized (Truelove, Grise Fiord) sites at select stations along near-to-offshore transects (see Figure 1), plotted by distance from the glacier terminus / shore. The individual bottle sample measurements are shown for nutrient (a-d) and total dissolvable metal (e,f) concentrations. Turbidity (g) and Chl *a* (i) data are from continuous sensor measurements through the water column. For euphotic zone depth (h), estimates (corresponding to 0.1% of surface PAR) at individual stations are shown. Note the log scale for Fe, Mn, turbidity and Chl *a*. Numbers of samples / stations are given in Table S2. Median, hinges, whiskers and outlier data are as described for Figure 2.

4.3 Variation across different glacier systems

Surface (upper 40 m) macronutrient concentrations within 10 km of the ice front also varied significantly ($p<0.05$; Table S4), and often systematically, across the different glacierized sites

(Figure 4). Belcher and Sydkap Glaciers represent the deepest tidewater glaciers we investigated (Table 1), and we find the highest average and median surface nitrate, phosphate, and silicate concentrations in proximate marine waters were associated with these sites. Belcher Glacier site median concentrations were $[NO_3^-]$ = 1.8 μM, $[PO_4^{3-}]$ = 0.51 μM, and $[SiO_4]$ = 4.9 μM, while Sydkap Glacier site median concentrations were $[NO_3^-]$ = 2.3 μM, $[PO_4^{3-}]$ = 0.50 μM, and $[SiO_4]$ = 6.0 μM. Comparatively, Sverdrup and Jakeman Glaciers have shallow submarine discharge depths (Table 1), and these sites showed variable trends with respect to macronutrient concentrations. Macronutrient concentrations at the Sverdrup Glacier site were relatively high and more similar to those at the Belcher and Sydkap Glacier sites compared to those at the Jakeman Glacier site (median concentrations at the Sverdrup Glacier site were $[NO_3^-]$ = 1.7 μM, $[PO_4^{3-}]$ = 0.42 μM, and $[SiO_4]$ = 4.2 μM). Macronutrient concentrations at the Jakeman Glacier site, in contrast, were comparable to the non-glacierized sites (median concentrations at the Jakeman Glacier site were $[NO_3^-]$ = 0.005 μM, $[PO_4^{3-}]$ = 0.36 μM, and $[SiO_4]$ = 1.6 μM). Jakeman Glacier has a slightly deeper estimated grounding line (-36 +/- 10 m a.s.l.) and larger estimated summer discharge (0.55 Gt/y) than Sverdrup Glacier (-21 +/- 10 m a.s.l. and 0.34 Gt/y). However, given the small proportion of Jakeman Glacier's calving front found in the water, a significant amount of its discharge is released first on land, rather than directly into the ocean. Notably, the first (bottle) station at the Jakeman Glacier site is further from the terminus (> 3 km) than at our other glacierized sites (≤ 1 km), which likely also accounts for differences we observed in macronutrient concentrations between the Sverdrup Glacier and Jakeman Glacier sites. Finally, we note that ammonia concentrations do not appear to systematically vary across our glacierized sites in a similar way to nitrate, phosphate and silicate concentrations. Instead, ammonia concentrations are similar across all of the glacierized sites. Ammonia was particularly enriched in waters proximate to Sydkap Glacier, where we observed a high density of seabird aggregation, which has previously been linked to elevated ammonium levels.

In general, total dissolvable metal micronutrients (TdFe, TdMn) in the surface ocean also varied systematically between our glacierized sites (Figure 4). We observed higher metal concentrations at the strongly-tidewater-glacier-influenced sites (Belcher Glacier site median concentrations were [Fe] = 1447 nM and [Mn] = 13 nM; Sydkap Glacier site median concentrations were [Fe] = 2017 nM and [Mn] = 51 nM; and Sverdrup Glacier site median concentrations were [Fe] = 13483 nM and [Mn] = 146 nM) compared to the weakly-tidewater-

543 glacier-influenced site (Jakeman Glacier site median concentrations were [Fe] = 1100 nM and
544 [Mn] = 15 nM). Notably, the maximum concentrations of TdFe and TdMn were very high at the
545 Belcher, Sydkap, and Sverdrup Glacier sites compared to those at the Jakeman Glacier site
546 (Figure 4), with ocean waters distal to Sverdrup Glacier, in particular, being especially enriched
547 (Figure 4). This is likely due to the fact that this was the only site where we could easily see the
548 plume at the surface, and as a result, extensively sampled it. In tandem with the total dissolvable
549 metals, turbidity was also higher, with much larger maximum values, at the Belcher, Sydkap, and
550 Sverdrup Glacier sites compared to at the Jakeman Glacier site.
551 Turbidity, light, and Chl *a* exhibited distinct patterns. Turbidity and light followed the
552 same systematic variation observed for the macronutrient and metal concentrations, showing
553 larger changes at the strongly-glacier-influenced sites relative to the weakly-glacier-influenced
554 site (Figure 4). The near-surface ocean within 10 km of the ice front of Belcher, Sydkap and
555 Sverdrup Glaciers was more turbid and had shallower euphotic zone depths compared to at the
556 Jakeman Glacier site (Wilcoxan Rank Sum Test, $p < 0.0001$). In contrast, Chl *a* concentrations
557 did not exhibit systematic trends across the different glacier systems (discussed below).
558

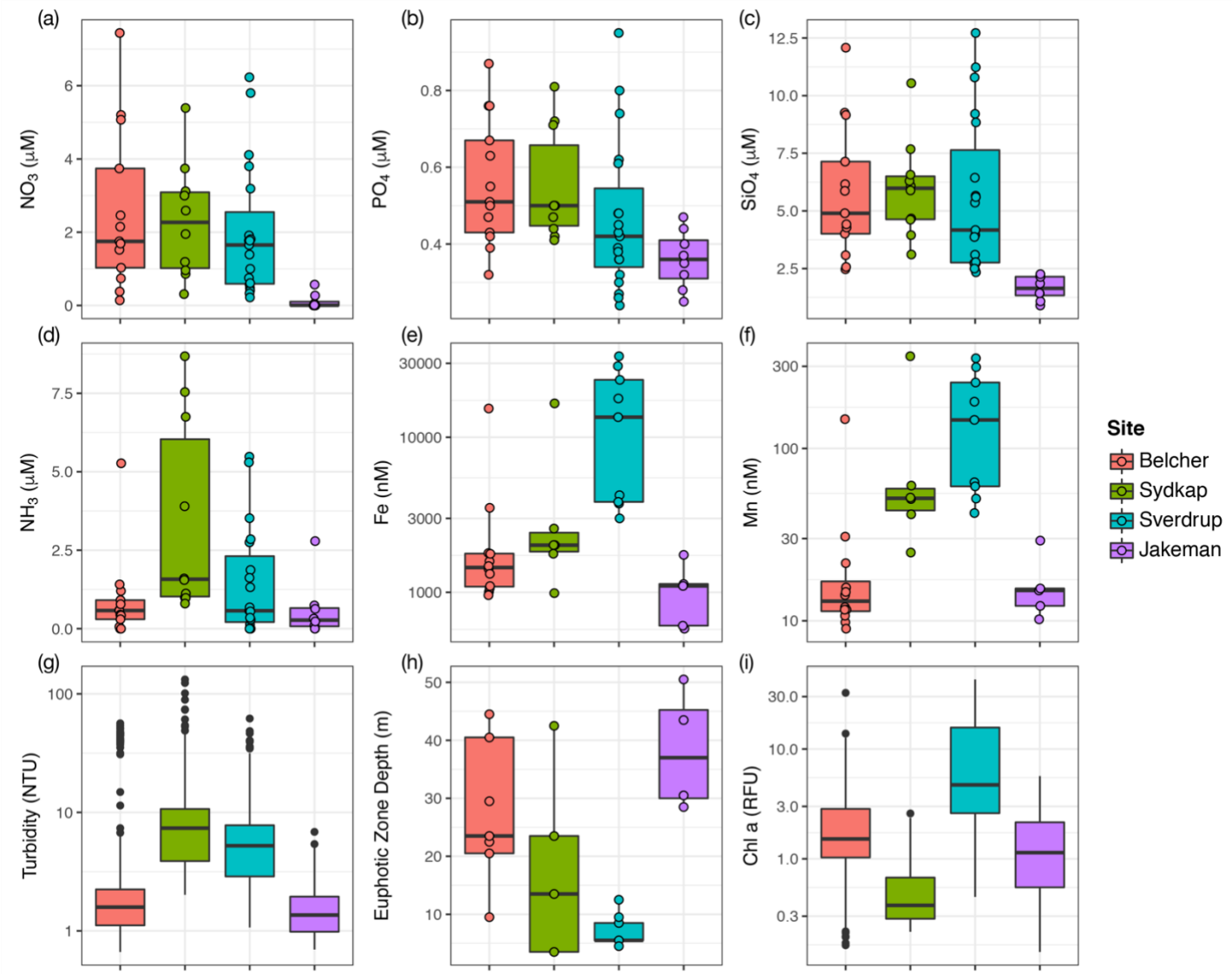

Figure 4. Comparisons of surface (upper 40 m) ocean water properties at tidewater glaciers in the CAA within 10-km of the ice front. Sites are organized by the estimated grounding line depth, with Belcher Glacier representing the deepest tidewater glacier considered and Jakeman Glacier representing a glacier in recession to a land-terminating system. The individual data points (corresponding to bottle samples at discrete depths) are shown for the nutrient (a-d) and total dissolvable metal (e,f) concentrations. Turbidity (g) and Chl *a* (i) data are from a continuous sensor measurement through the water column. Euphotic zone depth (h) was estimated at 0.1% of surface PAR at each station (individual data points). Note the log scale for Fe, Mn, turbidity and Chl *a*. Numbers of samples / stations are given in Table S2. Median, hinges, whiskers and outlier data are as described in Figure 2.

4.4 Interactions between turbidity, light, nutrients and chlorophyll a

The relationships observed between the vertical distributions of turbidity, light, nitrate and Chl *a* at the various glacierized and non-glacierized sites were varied and in some cases unexpected.

574 This is not surprising when considering the conflicting influences glacier meltwater input can
575 have on primary production: light availability can be restricted by the glacier-derived sediment
576 plume, which could limit phytoplankton growth, while the delivery of limiting nutrients (e.g.
577 NO_3^-; Figure S1) could enhance the growth of primary producers in the presence of sufficient
578 light. At the non-glacierized sites, Truelove Bay and Grise Fiord, we generally observed the
579 expected relationships between light, nitrate and Chl *a* in summer Arctic waters. Specifically,
580 vertical profiles showed a maxima in Chl *a* deeper in the water column where light was still
581 available and nitrate concentrations began to increase (Figure 5a and b). At the Jakeman Glacier
582 site, a weakly-glacier-influenced system, turbidity was low and light was plentiful, but the
583 relative lack of nitrate at stations in close proximity to the terminus (S4 and S6, ~4 km and 8 km
584 from the glacier terminus, respectively) may be limiting chlorophyll accumulation (Figure 5c).
585 At the Belcher and Sverdrup Glacier sites (Figure 5d and e), more strongly-glacier-influenced
586 systems, a turbid submarine discharge plume restricted light penetration, which appears to
587 influence Chl *a* distribution. At the station closest to the Belcher Glacier discharge (S10), the
588 presence of a large turbid plume is evident resulting in light attenuation throughout the water
589 column (Figure 5d). There is no peak in Chl *a* observed anywhere in the water column. Three
590 kilometers downstream at S11, the turbid plume is no longer observed and the euphotic zone
591 deepens, yet no increase in Chl *a* is evident. Interestingly, ~7 km from the glacier front at S13,
592 under similar light and nutrient conditions present at S11, a peak in Chl *a* is present ~20 m below
593 the surface. At the Sverdrup Glacier site (Figure 5e), the turbid plume is significantly shallower
594 than at the Belcher Glacier site and its presence is detected at ~ 1 and 4 km from the glacier front
595 (stations S22 and S27 respectively). Interestingly, peaks in Chl *a* are evident from within 1 km of
596 the glacier terminus to ~13 km out (S22, S27, S31) where there appears to be sufficient light and
597 nitrate present. However, peaks in Chl *a* occur below the calculated euphotic zone at all 3
598 stations, and within (S27) or below (S22) turbid waters (Figure 5e). This trend is also evident at
599 all the other stations (S23, S24, S25, S26, S28, S29, S30) sampled within 13 km of the Sverdrup
600 Glacier terminus (Polar Data Catalogue, Canadian Cryospheric Information Network (CCIN)
601 Reference No. 13211). Water column profiles from Sydkap Glacier showed elevated
602 macronutrient and ammonia concentrations in the presence of sufficient light, but no discernable
603 peak in Chl *a* (Figure 5f). This suggests that more complex biological and physical processes,
604 beyond the scope of our study, were impacting nutrient dynamics and productivity at this site.

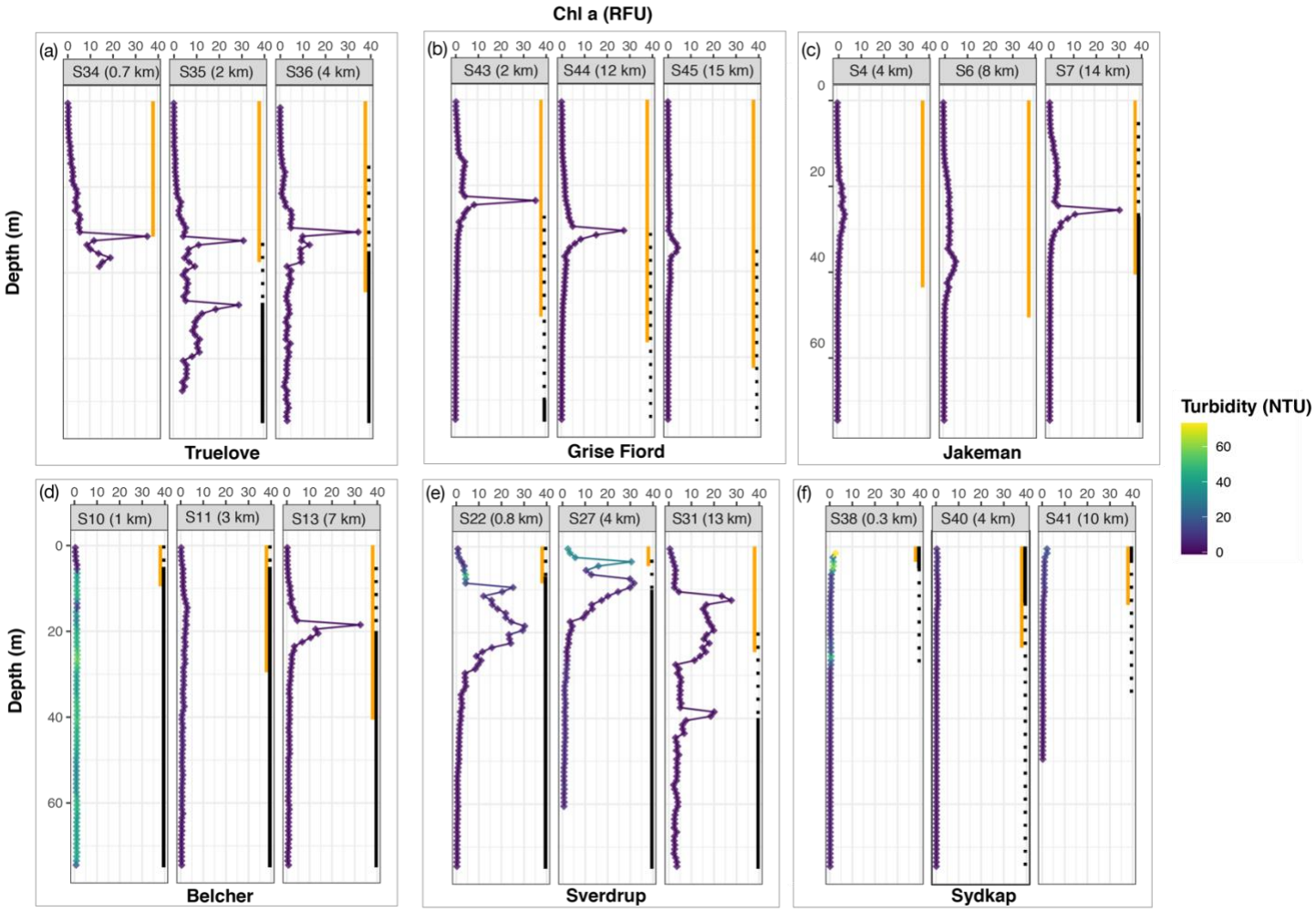

Figure 5. Vertical profiles of Chl *a* concentration (x-axis) and turbidity (color) measured at stations along marine transects emanating from the non-glacierized regions (a) Truelove, (b) Grise Fiord, and the glacierized sites at (c) Jakeman, (d) Belcher, (e) Sverdrup and (f) Sydkap Glaciers. The orange line shows the euphotic zone (to 0.1% surface PAR). The black line represents the depth range in which nitrate concentrations exceed 1 µM, with the dotted line indicating the range of depths in which this concentration threshold is reached. Subplots without a black line are those in which nitrate values above 1 µM were not detected in the upper 75-m of the water column. Station names (with distance from the glacier terminus / shore in parentheses) are given above each profile.

5 Discussion

5.1 Glaciers impact nutrient concentrations in the CAA coastal ocean

The effects of tidewater glaciers on marine nutrient availability in the euphotic zone of the ocean, and corresponding impacts up the food chain, have been the subject of speculation since the late

1930s (Cooper, 1952; Hartley & Dunbar, 1938; Vibe, 1939). In the last study on this topic in the CAA, Apollonio (1973) compared glacierized (South Cape Fiord) and non-glacierized (Grise Fiord) fjords in springtime, before sea ice melt. This study reported significantly higher nitrate concentrations in South Cape Fiord compared to Grise Fiord and open water in Jones Sound; whereas nitrate concentrations at the latter two sites were not significantly different. In contrast, he observed no statistically significant differences in phosphate or silica concentrations between the three sites. Despite this, Apollonio suggested that silica was likely present in significantly greater concentrations in the glacierized region. Building directly on this work, our comparison of nutrient concentrations in glacierized South Cape Fiord (i.e. in the proximity of Sydkap Glacier) and non-glacierized Grise Fiord in August 2019 illustrates a similar pattern of enhanced nitrate in the glacierized fjord (Apollonio, 1973). Our study expands these findings to include additional glacierized (in the proximity of Belcher, Sverdrup and Jakeman Glaciers) and non-glacierized (Truelove Bay) regions, and also demonstrates that the pattern of nitrate enhancement in glacierized regions extends to other macronutrients (phosphate, silicate) as well.

Though comparisons between adjacent glacierized and non-glacierized regions are sparse in the literature, the finding that surface marine waters in glacierized regions have enriched macronutrient (nitrate, phosphate, and silicate) concentrations (Figure 2), compared to typical Arctic surface ocean concentrations (Michel et al., 2006; Randelhoff et al., 2020), is consistent with recent results from Greenland and Svalbard fjords (Halbach et al., 2019; Kanna et al., 2018; Meire et al., 2017). However, the enrichments we observed here are generally much lower than those found in Greenlandic glacier systems. For example, at Bowdoin Glacier in northwest Greenland, where the subglacial discharge transects were conducted on a similar scale to this study, Kanna et al. (2018) report average nitrate (12.3 ± 0.6 (1 SD) μM), phosphate (1.0 ± 0.1μM), and silicate (12.3 ± 0.7 μM) concentrations in the plume surface waters that are much higher than those measured at any of the sites considered here in the CAA. Enrichment of this magnitude is not unique to the Bowdoin Glacier system: nitrate concentrations up to 12 μM were also observed in the upper 40-m of the water column within 10 km of the terminus of Narsap Sermia, a glacier draining into Godthabsfjord in southwest Greenland (Meire et al., 2017). Comparatively, average macronutrient concentrations observed by Halbach et al. (2019) in the surface (upper 10-m) waters of Kongsfjorden in the Svalbard archipelago, which has four smaller tidewater glaciers draining into it ($[NO_3^-]$ = 1.15 ± 0.39 μM, $[PO_4^{3-}]$ = 0.08 ± 0.03 μM, $[SiO_4]$ =

653 3.32 ± 0.33 μM), are similar to those observed here in the surface waters (upper 10-m) of the
654 glacierized sites in Jones Sound ($[NO_3^-]$ = 1.6 ± 1.5 μM, $[PO_4^{3-}]$ = 0.45 ± 0.16 μM, $[SiO_4]$ = 4.57
655 ± 2.79 μM). We propose that the similarity between the tidewater glaciers in this study and the
656 Svalbard archipelago glacier systems, rather than tidewater glaciers in Greenland, is likely
657 related to the mechanism by which macronutrients are being delivered to the surface waters of
658 glacierized regions (see Section 5.2).

659 The elevations in total dissolvable Fe and Mn in surface waters that we observe here are,
660 to our knowledge, the first measured in surface waters directly impacted by CAA tidewater
661 glaciers. However, such enrichments from glacial sources were hypothesized based on recently-
662 reported distributions of dissolved Mn and Fe in the broader CAA region (Colombo et al., 2020).
663 Others have also observed increases in Fe availability as a result of direct glacial input in
664 glacially-impacted systems in Greenland (Hawkings et al., 2018a; Hawkings et al., 2014; Kanna
665 et al., 2020) and Antarctica (Annett et al., 2017; Henkel et al., 2018). The spatially-variable and
666 highly-elevated TdFe concentrations we observe are consistent with these previous
667 measurements, and in fact appear to be among the highest such values reported to date
668 (Hopwood et al., 2019). TdFe was reported to be as high as 20 μM inside glacierized
669 Godthåbsfjord in southwest Greenland (Hopwood et al., 2018), compared to our > 30 μM values
670 within the Sverdrup Glacier plume waters. TdFe measurements from Sermilik Fjord, at the
671 margin of Helheim Glacier in southeast Greenland, show a 3-8 fold enhancement in surface
672 TdFe in the fjord and downstream (> 100 km from the glacier terminus) (Cape et al., 2018). Here
673 we observe enrichment in TdFe and TdMn (mean 10-fold increase over open Jones Sound
674 TdFe/TdMn between ~1-10 km of the ice terminus) that decreases as distance from the glacier
675 termini increases. Given our currently-limited understanding of the factors controlling metal
676 delivery, solubility, and persistence in glacier-ocean systems (Hopwood et al., 2019), it remains
677 challenging to put these first observations of metal micronutrient concentrations in CAA
678 glacierized regions into more complete context with other systems. These data do, however,
679 highlight the need for better spatial and chemical resolution of metal micronutrient dynamics in
680 these systems.
681
682 ***5.2 Mechanisms of nutrient delivery to the surface ocean***
683

Two different mechanisms have been put forward to account for the presence of elevated macronutrient concentrations in surface waters in the proximity of tidewater glacier fronts: (1) that glaciers deliver nutrients to the surface waters directly via nutrient-enriched runoff from the glacier (Beaton et al., 2017; Hawkings et al., 2016; Hendry et al., 2019) and (2) that the freshwater flux from marine-terminating glaciers causes deep seawater, which is rich in nutrients, to come to the surface with the rising submarine discharge plume (Hopwood et al., 2018; Kanna et al., 2018; Meire et al., 2017). While Apollonio (1973) hypothesized that the direct delivery of nutrient-enriched runoff resulted in the elevated macronutrient concentrations he observed at Sydkap Glacier in spring, the plume-upwelling mechanism has been shown to be important in numerous other similar glacier-ocean systems (Halbach et al., 2019; Kanna et al., 2018; Lydersen et al., 2014).

There are multiple indications that in our strongly-influenced tidewater glacier systems (i.e. Belcher and Sverdrup Glaciers), it is the upwelling of deeper, nutrient-rich seawater that underpins the elevated macronutrient concentrations observed. First, we see signatures of upwelling in the nearfield of the glacier termini in these systems in multiple fields mapped by the multi-channel logger measurements on transects emanating from the glacier calving front (Figure 6a and b). For example, at both the Belcher and Sverdrup sites, subsurface isopycnals tilt upwards toward the glacier front, as shown by the highlighted potential density anomaly surface of σ_θ= 26 kg/m^3. Consistently, low dissolved oxygen concentrations, characteristic of deeper waters, are seen in shallower sections of the water column at stations close to the glacier front. In contrast, at Jakeman Glacier (Figure 6c), a site not strongly influenced by tidewater glacier input, and at the non-glacierized sites (Figure 6d and e), isopycnals are relatively flat and upper ocean dissolved oxygen values remain relatively high, thus indicating a lack of upwelling of deeper waters. Notably though, our measurements from Jakeman Glacier begin at a distance from the terminus that may preclude us from observing stronger upwelling, were it present. Sydkap Glacier is anomalous, with no clear signature of upwelling detected (Dataset S2). We suspect this is due to insufficient resolution in our sensor measurements in this region, rather than an absence of upwelling. Our sampling resolution was likely insufficient here because this region (South Cape Fiord) appears to have a more complicated fjord circulation than our other study sites.

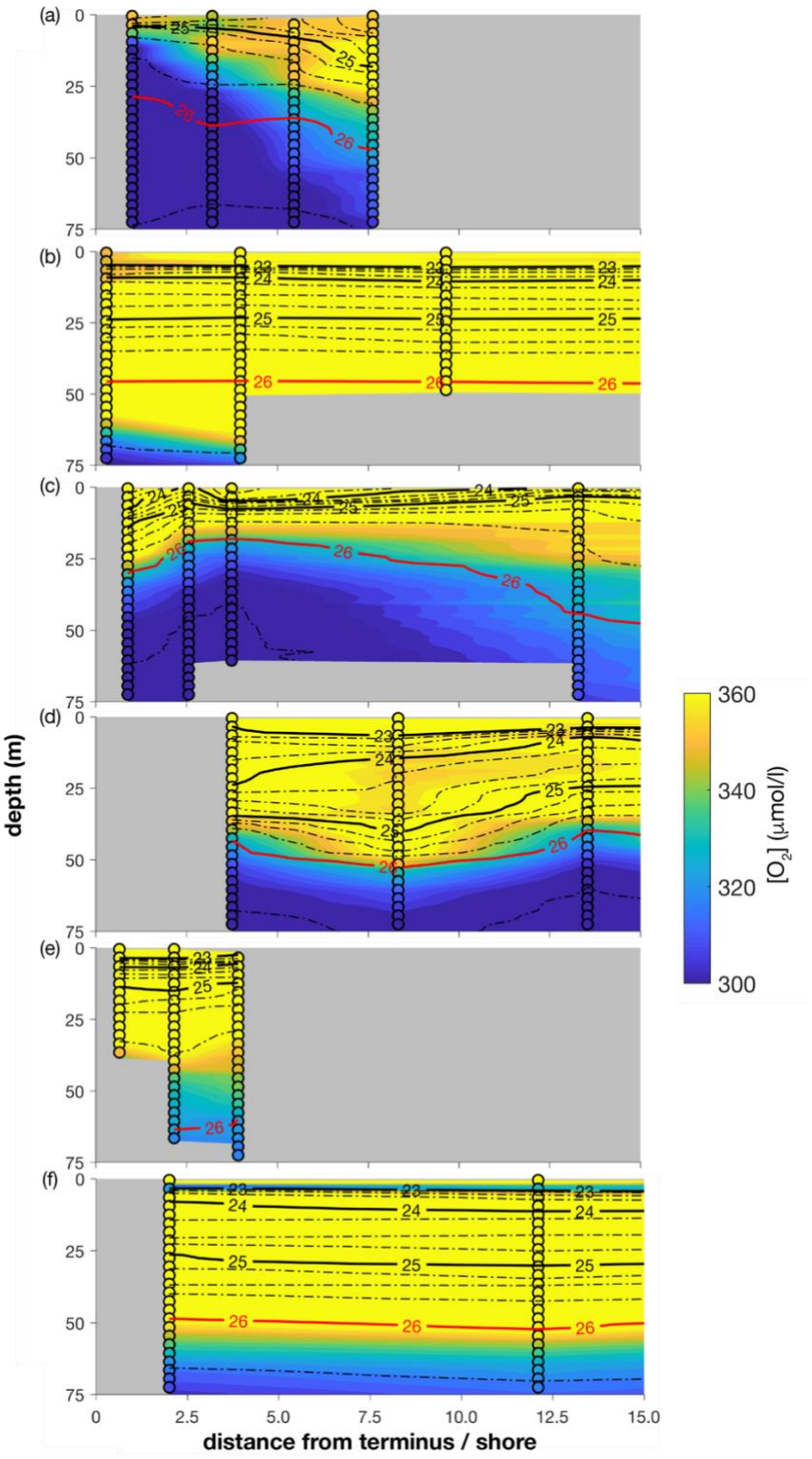

Figure 6. Section plots of dissolved oxygen concentration (color) and potential density anomaly (contour lines) for transects out from the termini of (a) Belcher, (b) Sydkap, (c) Sverdrup, and (d) Jakeman Glaciers as well as from the shore at (e) Truelove Bay and (f) Grise Fiord where no glaciers are present. Filled circles show points where profile data was collected colored by the direct (non-interpolated) measurement. The isopycnal used to calculate upwelling strength (Figure 8) is shown in red.

A further indication that enhanced macronutrient concentrations are sourced from deeper marine waters is found in an examination of the correlation of nutrient concentrations with apparent oxygen utilization (AOU) (Figure 7). AOU was calculated as described in Benson and Krause Jr. (1984) using the logger measurements of temperature, dissolved oxygen concentration and salinity, and is the difference between measured dissolved oxygen concentration and its equilibrium concentration at saturation. Positive AOU values can result from remineralization of organic matter, which consumes oxygen and generates macronutrients. A positive correlation between AOU and macronutrient concentrations suggests that nutrient concentrations and AOU are influenced by the same processes. Strong positive linear relationships (Pearson correlation, $p < 0.01$) between AOU and macronutrient concentrations, observed at all three strongly-influenced glacierized sites (Belcher, Sydkap, and Sverdrup Glaciers), suggests that in these systems, remineralization in deeper marine waters is a significant macronutrient source. Further, a lack of correlation between AOU and turbidity (Figure 7), which is supplied by glacier input directly and enriched in low-density water, suggests macronutrients are not appreciably supplied via direct glacial input.

Notably, TdFe and TdMn concentrations are not correlated with AOU, and instead display very similar distributions to turbidity (Figure 7). This suggests that these micronutrients are, in contrast to macronutrients, supplied directly from glacier discharge. This conclusion is consistent with the result that variations in macronutrient concentrations across the different sites show a different pattern to variations in TdFe and TdMn concentrations, turbidity and light availability (Figure 4). Further, it is also evident, based on depth profiles of these metals (Figure S2), that upwelled deep water would not be enriched in TdFe or TdMn, and so could not be the source to the upper water column. The distinction between the proposed delivery mechanisms of macro- vs micro-nutrients in these systems is significant, as it may imply differing dependencies on glacial forcing parameters as well as differing sensitivities to change.

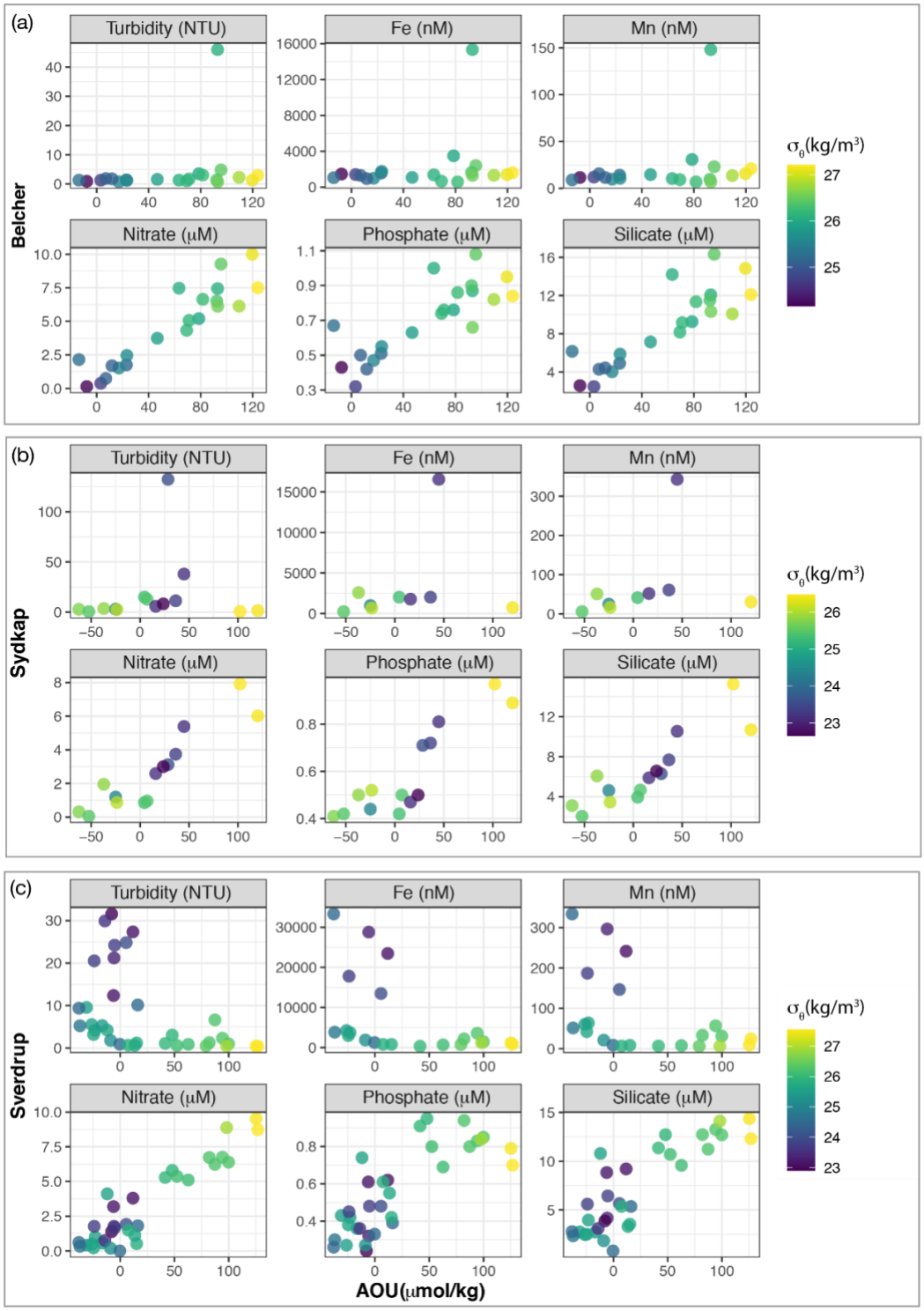

Figure 7. Apparent oxygen utilization (AOU) versus turbidity, TdFe, TdMn, and nitrate (NO_3^-), phosphate (PO_4^{3-}), and silicate (SiO_4^-) concentrations in the marine waters at (a) Belcher (b) Sydkap and (c) Sverdrup Glaciers. The color scale indicates potential density anomaly in the water column. Positive linear relationships were assessed using a Pearson correlation and were significant ($p < 0.05$) between AOU and major macronutrient concentrations along each transect. Positive linear correlations between AOU and turbidity, TdFe, and TdMn were not significant ($p > 0.05$).

5.3 Influence of tidewater glaciers on factors driving marine primary production

Though the presence of glaciers in Jones Sound clearly impacts factors that drive primary productivity, potential effects on phytoplankton growth are complex. This is not surprising considering the interplay of physical and biological processes affecting Chl *a* concentrations in our study sites, including light attenuation in sediment-laden meltwater plumes, fjord/estuarine filter effects, plankton nutritional status, and microbial nutrient and carbon utilisation pathways. Ultimately, primary productivity in glacial fjords is a balance between all of these varying influences. In the Arctic summer, when light is plentiful, standing nutrient stocks will be drawn down by primary producers in the euphotic zone unless replenished (Randelhoff et al., 2020). In our study, this drawdown is evident in the lower nutrient concentrations observed at the non-glacierized sites (Truelove Bay and Grise Fiord) and at Jakeman Glacier, a system weakly influenced by tidewater glacier input. The higher micro- and macro-nutrient concentrations observed at the glacierized sites point to either a lack of drawdown due to limited light penetration in the meltwater plumes or a mechanism for nutrient replenishment continually present throughout the summer. Given that we have documented upwelling of nitrate-enriched waters co-located with elevated surface nitrate levels, glacier-driven replenishment by upwelling appears to play an important role in the observed elevated macronutrient concentrations. The absence of enhanced Chl *a* concentrations close to the glacier fronts (e.g. at Belcher Glacier) is not surprising given light attenuation caused by the suspended sediments in the rising glacial meltwater plume. Previous studies in Greenland and Alaska have noted that Chl *a* concentrations and primary productivity measurements are typically highest distal (> 20 km) to the ice front, once a significant proportion of glacially-derived silt has settled out and the euphotic zone depth has increased (Etherington et al., 2007; Meire et al., 2017). Thus, a “goldilocks zone” outside of the turbid plume but proximal to the ice edge where the nutritive benefits of the plume can still be experienced by *in situ* phytoplankton has been found to be typical in Greenlandic and Alaskan glacierized fjords (Kanna et al., 2018; Meire et al., 2017). However, in smaller glacial systems, such as in the Svalbard (Halbach et al., 2019) or as shown here in the CAA, this zone might exist closer to the glacier front.

784 The locally-elevated macronutrient concentrations observed here are likely most
785 impactful in waters just downstream from these glacier systems. However, the metal
786 contributions we observed have the potential to impact productivity regionally. While
787 phytoplankton growth in the CAA is unlikely to be limited by micronutrient availability, regions
788 downstream, including the Labrador Sea, can have areas of extremely low metal concentrations
789 (Colombo et al 2020), and thus have the potential to be impacted by enhanced metal delivery
790 from upstream CAA glacier sources. While some of the elevated TdFe and TdMn in these glacier
791 systems will be subject to estuarine removal (Schroth et al., 2014), given the extremely high
792 TdFe and TdMn values we observed here, previous observations of elevated DFe and DMn
793 concentrations adjacent to CAA glacier systems (Colombo et al., 2020), and signatures of
794 elevated metal availability 10s to 100s of kilometers from glaciers in other systems (Hopwood et
795 al., 2019), these contributions may indeed influence metal availability in recipient seas. Notably,
796 the Labrador Sea contains regions that bear signatures of elevated metal concentrations, which
797 may be associated with glacier and/or shelf-derived sources (Colombo et al., 2020; Tonnard et
798 al., 2020). Studies in the North Atlantic also note high Fe, Mn and other metal concentrations
799 associated with Labrador Sea water masses: these may be consistent with a glacier source,
800 though this requires further investigation (Conway & John, 2014; Noble et al., 2017). A portion
801 of glacier-derived metal signatures is likely to be highly bioavailable as nanoparticulate iron, as
802 observed in other glacial systems (Hawkings et al., 2018a; Hawkings et al., 2014). The
803 partitioning of these metal contributions into different chemical phases that are more or less
804 likely to remain in solution or suspension for long-range transport are likely to be strongly
805 impacted by the organic environment in which they are delivered and processed (Zhang et al.,
806 2015), as well as by possible benthic recycling (Wehrmann et al., 2014). As such, future work is
807 required to examine the role of this metal delivery in shaping micronutrient bioavailability
808 locally and regionally.
809
810
811 **6 Conclusions**
812
813 In the first assessment of glacier-ocean interactions in the CAA in 50 years, we use Jones Sound
814 as a natural laboratory to examine the role of glaciers in marine biogeochemistry, exploiting its

continuum of tidewater glacierized, partially tidewater glacierized, and non-glacierized sites. To summarize key aspects of these interactions, we examine the relationship between tidewater subglacial discharge, a metric of observed upwelling strength, and euphotic zone nutrient enrichment (Figure 8). This analysis, excluding Sydkap Glacier for reasons described above, reveals a significant correlation (Pearson correlation coefficient) between tidewater discharge volume and upwelling strength ($p = 0.004$), as well as nitrate enrichment ($p = 0.02$). This suggests that the volume of water discharged sub-glacially is an important determinant of the strength of upwelling and macronutrient delivery to the euphotic zone. However, the degree of macronutrient enrichment will also depend directly on macronutrient concentrations in the water column at the depth of glacial discharge (Hopwood et al., 2018; Oliver et al., 2020). Our results indicate that even glaciers with shallow grounding lines, provided they have sufficient glacial discharge below the marine nutricline, can enhance delivery of macronutrients to near-surface waters (Halbach et al., 2019; Williams et al., submitted). Unlike macronutrient concentrations, however, a correlation between surface water total dissolvable metal micronutrient enrichment and tidewater discharge volume does not exist (data not shown), highlighting that there is considerable work to be done to understand the factors (geological, glacial, biological, and oceanographic) that control metal delivery to surface waters in glacial systems.

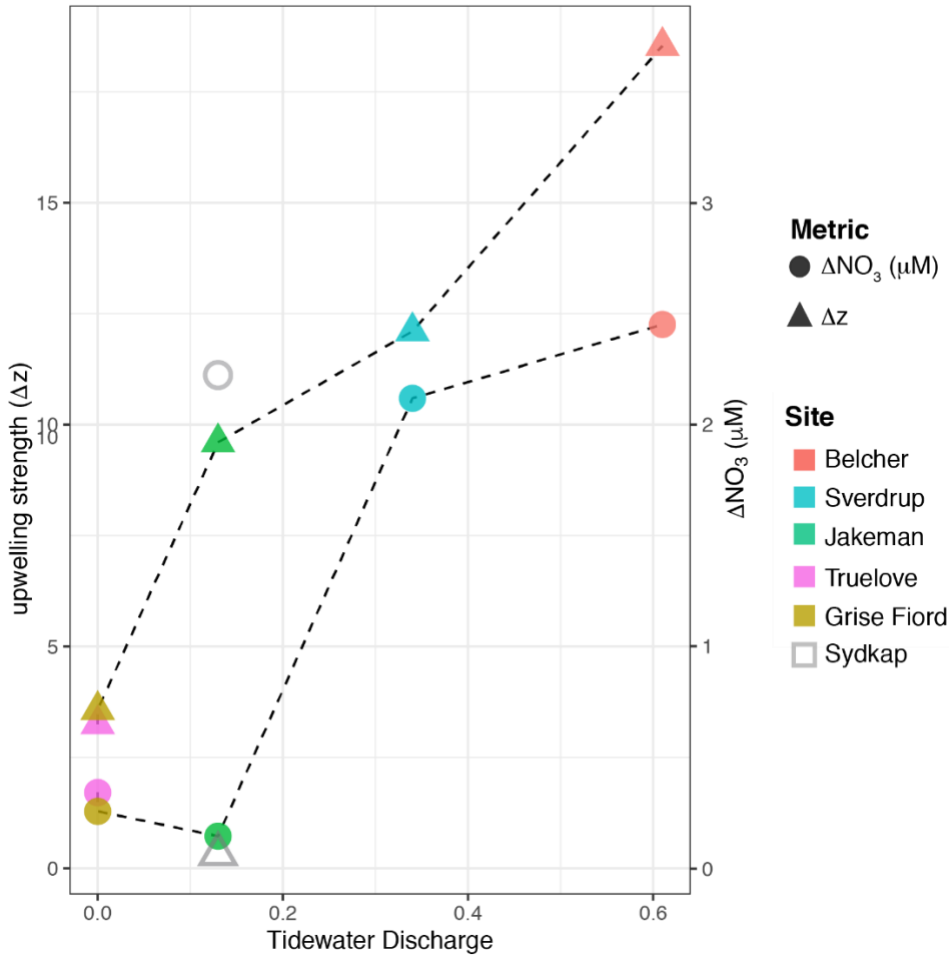

Figure 8. Relationships between annual tidewater discharge (modeled discharge in Table 1 scaled by the fraction of the glacier terminus that interfaces with the ocean), a metric of upwelling strength, Δz (the change in depth of the 1026 kg/m^3 isopycnal from open water in Jones Sound to within 12-km of the terminus / shore), and a metric of euphotic zone nutrient enrichment, Δ nitrate (the change in average nitrate concentration from open water in Jones Sound to within 12-km of the terminus/shore). Sydkap Glacier, showing anomalous relationships to the other systems, is shown in grey open symbols.

Glaciers in the CAA, and their associated impacts on the marine environment, are vulnerable to change (Cook et al., 2019). In the future, as they retreat, the discharge point of these glaciers will change. Many tidewater glaciers in the CAA (e.g. Sverdrup Glacier) are situated on retrograde bed slopes, meaning that their termini will remain below sea-level even with kilometer-scale retreat. Owing to their bed slope geometry, these glaciers will likely exhibit a deepening of the depth at which their submarine freshwater discharge is released in the ocean as they retreat on this scale. Conversely, the discharge depths of glaciers on prograde slopes (e.g. Sydkap Glacier) will likely exhibit a shoaling with glacier retreat. In the short term, submarine discharge released at shallower, yet still below the nutricline, depths in the ocean will enable

macronutrients entrained by the buoyant plume to reach the surface (Halbach et al., 2019). Additionally, with increased climate warming, longer melt seasons may increase the number and temporal consistency of plumes released at the glacier terminus, resulting in smaller but more consistent upwelling (Halbach et al., 2019). However, inevitably, with continued melt, glaciers that terminate in the ocean will cross a grounding line threshold and become land-terminating (expected first for systems like Jakeman Glacier), shifting their discharge point to the ocean surface. Our observations suggest that such changes will result in the loss of the glacier-driven upwelling of limiting macronutrients to the euphotic zone along CAA coastlines, and may further reduce nutrient delivery to the surface as a result of enhanced stratification. However, as glacial discharges grow and then shrink as melt accelerates, it is possible that metal delivery to the oceans will scale similarly. Given the extremely large inputs of metal micronutrients detected here, and the importance of metal micronutrients for productivity in downstream environments in the North Atlantic (Achterberg et al., 2018), constraining the processes controlling metal fate and bioavailability in these systems, and how they may respond to change, is critical. Additional focus is also required to develop predictive models of the cumulative impact of glaciers in the CAA on both local and regional primary productivity in the face of climate change.

Acknowledgements

We thank Jimmy Qaapik, the Hamlet of Grise Fiord, the Brossier Family, Andrew Hamilton and the Polar Continental Shelf Project (PCSP) for invaluable assistance in the field. We acknowledge financial support from NFRF Explorations Fund Grant NFRFE-2018-01427 to E. Bertrand, S. Waterman, M. Bhatia, and J. Qaapik, NSERC Shiptime (RGPST-544982-2020) to J. Halfar and P. Myers, PCSP grant 68719 to M. Bhatia, Canada Research Chair funding to E. Bertrand and S. Waterman, and Campus Alberta Innovation Program Chair funding to M. Bhatia. Support for D. Burgess was provided by the Climate Change Geoscience Program, Lands and Minerals Sector, Natural Resources Canada. We are also grateful to Martin Sharp for illuminating discussions.

Data Availability Statement

An electronic copy of the *in situ* oceanographic measurements (conductivity, temperature, pressure, dissolved oxygen, photosynthetic active radiation, chlorophyll *a* (Chl *a*), and turbidity) from this study is available online at Polar Data Catalogue (CCIN Reference No. 13211).

Contributions

E. Bertrand, M. Bhatia, D. Burgess, and S. Waterman designed the study. E. Bertrand, M. Bhatia, and D. Burgess completed the field work. P. Williams calculated the RACMO v2-derived glacier characteristics and P. Williams and M. Roberts analyzed the macronutrient data. R. Bundy and T. Mellett analyzed and helped interpret the trace metal data. All authors contributed to making the figures and writing the manuscript.

References

Achterberg, E. P., Steigenberger, S., Marsay, C. M., LeMoigne, F. A. C., Painter, S. C., Baker, A. R., et al. (2018). Iron Biogeochemistry in the High Latitude North Atlantic Ocean. *Sci Rep, 8*(1), 1283. doi:10.1038/s41598-018-19472-1

Annett, A. L., Fitzsimmons, J. N., Séguret, M. J. M., Lagerström, M., Meredith, M. P., Schofield, O., & Sherrell, R. M. (2017). Controls on dissolved and particulate iron distributions in surface waters of the Western Antarctic Peninsula shelf. *Marine Chemistry, 196*, 81-97. doi:10.1016/j.marchem.2017.06.004

Apollonio, S. (1973). Glaciers and Nutrients in Arctic Seas. *Science 180*(4085), 491-493.

Arrigo, K. R., van Dijken, G. L., Castelao, R. M., Luo, H., Rennermalm, Å. K., Tedesco, M., et al. (2017). Melting glaciers stimulate large summer phytoplankton blooms in southwest Greenland waters. *Geophysical Research Letters, 44*(12), 6278-6285. doi:10.1002/2017gl073583

Barber, F. G., & Huyer, A. (1977). *On the oceanography of Jones Sound, NWT*. Ottawa, Ontario, Canada.

Batchelor, C. L., Dowdeswell, J. A., Dowdeswell, E. K., Todd, B. J., & Sharp, M. J. (2016). A tidewater glacier landform assemblage in Belcher Inlet, Canadian Arctic. *Geological Society, London, Memoirs, 46*(1), 155-158. doi:10.1144/m46.146

Beaton, A. D., Wadham, J. L., Hawkings, J., Bagshaw, E. A., Lamarche-Gagnon, G., Mowlem, M. C., & Tranter, M. (2017). High-Resolution in Situ Measurement of Nitrate in Runoff from the Greenland Ice Sheet. *Environmental Science & Technology, 51*(21), 12518-12527. doi:10.1021/acs.est.7b03121

Benson, B. B., & Krause Jr., D. (1984). The concentration and isotopic fractionation of oxygen dissolved in freshwater and seawater in equilibrium with the atmosphere1. *Limnology and Oceanography, 29*(3), 620-632. doi:https://doi.org/10.4319/lo.1984.29.3.0620

Bhatia, M. P., Kujawinski, E. B., Das, S. B., Breier, C. F., Henderson, P. B., & Charette, M. A. (2013). Greenland meltwater as a significant and potentially bioavailable source of iron to the ocean. *Nature Geoscience, 6*(4), 274-278. doi:10.1038/ngeo1746

Bliss, A., Hock, R., & Radić, V. (2014). Global response of glacier runoff to twenty-first century climate change. *Journal of Geophysical Research: Earth Surface, 119*(4), 717-730. doi:10.1002/2013jf002931

Boon, S., Burgess, D. O., Koerner, R. M., & Sharp, M. J. (2010). Forty-seven Years of Research on the Devon Island Ice Cap, Arctic Canada. *Arctic, 63*(1), 13-29.

Box, J. E., Colgan, W. T., Wouters, B., Burgess, D. O., O'Neel, S., Thomson, L. I., & Mernild, S. H. (2018). Global sea-level contribution from Arctic land ice: 1971–2017. *Environmental Research Letters, 13*(12). doi:10.1088/1748-9326/aaf2ed

Boyle, E. A., Edmond, J. M., & Sholkovitz, E. R. (1977). The mechanism of iron removal in estuaries. *Geochimica et Cosmochimica Acta, 41*(9), 1313-1324. doi:https://doi.org/10.1016/0016-7037(77)90075-8

Burgess, D. O., & Sharp, M. J. (2004). Recent Changes in Areal Extent of the Devon Ice Cap, Nunavut, Canada. *Arctic, Antarctic, and Alpine Research, 36*(2), 261-271. doi:10.1657/1523-0430(2004)036[0261:Rciaeo]2.0.Co;2

Burgess, D. O., Sharp, M. J., Mair, D. W. F., Dowdeswell, J. A., & Benham, T. J. (2005). Flow dynamics and iceberg calving rates of Devon Ice Cap, Nunavut, Canada. *Journal of Glaciology, 51*(173), 219-230.

939 Cantoni, C., Hopwood, M. J., Clarke, J. S., Chiggiato, J., Achterberg, E. P., & Cozzi, S. (2020).
940 Glacial Drivers of Marine Biogeochemistry Indicate a Future Shift to More Corrosive
941 Conditions in an Arctic Fjord. *Journal of Geophysical Research: Biogeosciences, 125*(11). doi:10.1029/2020jg005633
942 Cape, M. R., Straneo, F., Beaird, N., Bundy, R. M., & Charette, M. A. (2018). Nutrient release to
943 oceans from buoyancy-driven upwelling at Greenland tidewater glaciers. *Nature Geoscience, 12*(1), 34-39. doi:10.1038/s41561-018-0268-4
944
945
946 Carroll, D., Sutherland, D. A., Hudson, B., Moon, T., Catania, G. A., Shroyer, E. L., et al.
947 (2016). The impact of glacier geometry on meltwater plume structure and submarine melt
948 in Greenland fjords. *Geophysical Research Letters, 43*(18), 9739-9748.
949 doi:10.1002/2016gl070170
950 Catania, G. A., Stearns, L. A., Sutherland, D. A., Fried, M. J., Bartholomaus, T. C., Morlighem,
951 M., et al. (2018). Geometric Controls on Tidewater Glacier Retreat in Central Western
952 Greenland. *Journal of Geophysical Research: Earth Surface, 123*(8), 2024-2038.
953 doi:10.1029/2017jf004499
954 Colombo, M., Jackson, S. L., Cullen, J. T., & Orians, K. J. (2020). Dissolved iron and
955 manganese in the Canadian Arctic Ocean: On the biogeochemical processes controlling
956 their distributions. *Geochimica et Cosmochimica Acta, 277*, 150-174.
957 doi:10.1016/j.gca.2020.03.012
958 Conway, T. M., & John, S. G. (2014). Quantification of dissolved iron sources to the North
959 Atlantic Ocean. *Nature, 511*(7508), 212-215. doi:10.1038/nature13482
960 Cook, A. J., Copland, L., Noël, B. P. Y., Stokes, C. R., Bentley, M. J., Sharp, M. J., et al. (2019).
961 Atmospheric forcing of rapid marine-terminating glacier retreat in the Canadian Arctic
962 Archipelago. *Science Advances, 5*(3), eaau8507. doi:10.1126/sciadv.aau8507
963 Cooper, L. H. N. (1952). Factors affecting the distribution of silicate in the Northern Atlantic
964 Ocean and the formation of North Atlantic deep water. *J. mar. biol. Ass. U. K., 30*, 511-
965 526.
966 Copland, L., Sharp, M. J., & Dowdeswell, J. A. (2003). The distribution and flow characteristics
967 of surge-type glaciers in the Canadian High Arctic. *Annals of Glaciology, 36*, 73-81.
968 doi:10.3189/172756403781816301
969 Cress, P., & Wyness, R. (1961). The Devon Island expedition, observations of glaical
970 movements. *Arctic, 14*(4), 257-259.
971 Cutter, G. A., & Bruland, K. W. (2012). Rapid and noncontaminating sampling system for trace
972 elements in global ocean surveys. *Limnology and Oceanography: Methods, 10*(6), 425-
973 436. doi:10.4319/lom.2012.10.425
974 Danielson, B., & Sharp, M. (2017). Development and application of a time-lapse photograph
975 analysis method to investigate the link between tidewater glacier flow variations and
976 supraglacial lake drainage events. *Journal of Glaciology, 59*(214), 287-302.
977 doi:10.3189/2013JoG12J108
978 Dowdeswell, J. A., Benham, T. J., Gorman, M. R., Burgess, D., & Sharp, M. J. (2004). Form and
979 flow of the Devon Island Ice Cap, Canadian Arctic. *Journal of Geophysical Research: Earth Surface, 109*(F2), n/a-n/a. doi:10.1029/2003jf000095
980
981 Etherington, L. L., Hooge, P. N., Hooge, E. R., & Hill, D. F. (2007). Oceanography of Glacier
982 Bay, Alaska: Implications for Biological Patterns in a Glacial Fjord Estuary. *Estuaries and Coasts, 30*(6), 927-944.
983

Everett, A., Kohler, J., Sundfjord, A., Kovacs, K. M., Torsvik, T., Pramanik, A., et al. (2018). Subglacial discharge plume behaviour revealed by CTD-instrumented ringed seals. *Sci Rep, 8*(1), 13467. doi:10.1038/s41598-018-31875-8

Fransson, A., Chierici, M., Nomura, D., Granskog, M. A., Kristiansen, S., Martma, T., & Nehrke, G. (2015). Effect of glacial drainage water on the CO2 system and ocean acidification state in an Arctic tidewater-glacier fjord during two contrasting years. *Journal of Geophysical Research: Oceans, 120*(4), 2413-2429. doi:https://doi.org/10.1002/2014JC010320

Gardner, A. S., Moholdt, G., Wouters, B., Wolken, G. J., Burgess, D. O., Sharp, M. J., et al. (2011). Sharply increased mass loss from glaciers and ice caps in the Canadian Arctic Archipelago. *Nature, 473*(7347), 357-360. doi:10.1038/nature10089

Gogineni, S., Tammana, D., Braaten, D., Leuschen, C., Akins, T., Legarsky, J., et al. (2001). Coherent radar ice thickness measurements over the Greenland ice sheet. *Journal of Geophysical Research: Atmospheres, 106*(D24), 33761-33772. doi:10.1029/2001jd900183

Greisman, P. (1979). On upwelling driven by the melt of ice shelves and tidewater glaciers. *Deep Sea Research Part A Oceanography Research Papers, 26*(9), 1051-1065.

Halbach, L., Vihtakari, M., Duarte, P., Everett, A., Granskog, M. A., Hop, H., et al. (2019). Tidewater Glaciers and Bedrock Characteristics Control the Phytoplankton Growth Environment in a Fjord in the Arctic. *Frontiers in Marine Science, 6*. doi:10.3389/fmars.2019.00254

Harrison, J. C., Thorsteinsson, R., Frisch, T., Mayr, U., Gilbert, C., Lynds, T., & Ford, A. (Cartographer). (2015). Geology, Tectonic assemblage map of Grise Fiord, eastern Devon and southern Ellesmere islands, Nunavut

Hartley, A., & Dunbar, G. (1938). On the hydrographic mechanism of the so-called brown zones associated with tidal glaciers. *Journal of Marine Research, 1*, 305-311.

Hawkings, J., Wadham, J., Tranter, M., Telling, J., Bagshaw, E., Beaton, A., et al. (2016). The Greenland Ice Sheet as a hot spot of phosphorus weathering and export in the Arctic. *Global Biogeochemical Cycles, 30*(2), 191-210. doi:10.1002/2015gb005237

Hawkings, J. R., Benning, L. G., Raiswell, R., Kaulich, B., Araki, T., Abyaneh, M., et al. (2018a). Biolabile ferrous iron bearing nanoparticles in glacial sediments. *Earth and Planetary Science Letters, 493*, 92-101. doi:10.1016/j.epsl.2018.04.022

Hawkings, J. R., Hatton, J. E., Hendry, K. R., de Souza, G. F., Wadham, J. L., Ivanovic, R., et al. (2018b). The silicon cycle impacted by past ice sheets. *Nat Commun, 9*(1), 3210. doi:10.1038/s41467-018-05689-1

Hawkings, J. R., Wadham, J. L., Benning, L. G., Hendry, K. R., Tranter, M., Tedstone, A., et al. (2017). Ice sheets as a missing source of silica to the polar oceans. *Nat Commun, 8*, 14198. doi:10.1038/ncomms14198

Hawkings, J. R., Wadham, J. L., Tranter, M., Lawson, E., Sole, A., Cowton, T., et al. (2015). The effect of warming climate on nutrient and solute export from the Greenland Ice Sheet. *Geochemical Perspectives Letters, 1*, 94-104. doi:http://dx.doi.org/10.7185/geochemlet.1510

Hawkings, J. R., Wadham, J. L., Tranter, M., Raiswell, R., Benning, L. G., Statham, P. J., et al. (2014). Ice sheets as a significant source of highly reactive nanoparticulate iron to the oceans. *Nat Commun, 5*, 3929. doi:10.1038/ncomms4929

1029 Hendry, K. R., Huvenne, V. A. I., Robinson, L. F., Annett, A., Badger, M., Jacobel, A. W., et al.
1030 (2019). The biogeochemical impact of glacial meltwater from Southwest Greenland.
1031 *Progress in Oceanography, 176*. doi:10.1016/j.pocean.2019.102126
1032 Henkel, S., Kasten, S., Hartmann, J. F., Silva-Busso, A., & Staubwasser, M. (2018). Iron cycling
1033 and stable Fe isotope fractionation in Antarctic shelf sediments, King George Island.
1034 *Geochimica et Cosmochimica Acta, 237*, 320-338. doi:10.1016/j.gca.2018.06.042
1035 Holding, J. M., Markager, S., Juul-Pedersen, T., Paulsen, M. L., Møller, E. F., Meire, L., & Sejr,
1036 M. K. (2019). Seasonal and spatial patterns of primary production in a high-latitude fjord
1037 affected by Greenland Ice Sheet run-off. *Biogeosciences, 16*(19), 3777-3792.
1038 doi:10.5194/bg-16-3777-2019
1039 Hood, E., & Scott, D. (2008). Riverine organic matter and nutrients in southeast Alaska affected
1040 by glacial coverage. *Nature Geoscience, 1*(9), 583-587. doi:10.1038/ngeo280
1041 Hopwood, M. J., Carroll, D., Browning, T. J., Meire, L., Mortensen, J., Krisch, S., & Achterberg,
1042 E. P. (2018). Non-linear response of summertime marine productivity to increased
1043 meltwater discharge around Greenland. *Nat Commun, 9*(1), 3256. doi:10.1038/s41467-
1044 018-05488-8
1045 Hopwood, M. J., Carroll, D., Dunse, T., Hodson, A., Holding, J. M., Iriarte, J. L., et al. (2019).
1046 How does glacier discharge affect marine biogeochemistry and primary production in the
1047 Arctic? . *The Cryosphere, 136*. doi:10.5194/tc-2019-136
1048 Juul-Pedersen, T., Arendt, K. E., Mortensen, J., Blicher, M. E., Søgaard, D. H., & Rysgaard, S.
1049 (2015). Seasonal and interannual phytoplankton production in a sub-Arctic tidewater
1050 outlet glacier fjord, SW Greenland. *Marine Ecology Progress Series, 524*, 27-38.
1051 doi:10.3354/meps11174
1052 Kanna, N., Sugiyama, S., Fukamachi, Y., Nomura, D., & Nishioka, J. (2020). Iron Supply by
1053 Subglacial Discharge Into a Fjord Near the Front of a Marine-Terminating Glacier in
1054 Northwestern Greenland. *Global Biogeochemical Cycles, 34*(10).
1055 doi:10.1029/2020gb006567
1056 Kanna, N., Sugiyama, S., Ohashi, Y., Sakakibara, D., Fukamachi, Y., & Nomura, D. (2018).
1057 Upwelling of Macronutrients and Dissolved Inorganic Carbon by a Subglacial Freshwater
1058 Driven Plume in Bowdoin Fjord, Northwestern Greenland. *Journal of Geophysical*
1059 *Research: Biogeosciences, 123*(5), 1666-1682. doi:10.1029/2017jg004248
1060 Keefer, B. J., Smith, J. L., & Gregoire, T. G. (1991). Modeling and evaluating the effects of
1061 stream mode digitizing errors on map variables. *Photogrammetric engineering and*
1062 *remote sensing, 57*(7), 957-963.
1063 King, M. D., Howat, I. M., Candela, S. G., Noh, M. J., Jeong, S., Noël, B. P. Y., et al. (2020).
1064 Dynamic ice loss from the Greenland Ice Sheet driven by sustained glacier retreat.
1065 *Communications Earth & Environment, 1*(1). doi:10.1038/s43247-020-0001-2
1066 Krisch, S., Browning, T. J., Graeve, M., Ludwichowski, K. U., Lodeiro, P., Hopwood, M. J., et
1067 al. (2020). The influence of Arctic Fe and Atlantic fixed N on summertime primary
1068 production in Fram Strait, North Greenland Sea. *Sci Rep, 10*(1), 15230.
1069 doi:10.1038/s41598-020-72100-9
1070 Lydersen, C., Assmy, P., Falk-Petersen, S., Kohler, J., Kovacs, K. M., Reigstad, M., et al.
1071 (2014). The importance of tidewater glaciers for marine mammals and seabirds in
1072 Svalbard, Norway. *Journal of Marine Systems, 129*, 452-471.
1073 doi:10.1016/j.jmarsys.2013.09.006

McDougall, T. J., & Barker, P. M. (2011). *Getting started with TEOS-10 and the Gibbs Seawater (GSW) Oceanographic Toolbox* (ISBN 978-0-646-55621-5). Retrieved from

McGrath, T., Cronin, M., Kerrigan, E., Wallace, D., Gregory, C., Normandeau, C., & McGovern, E. (2019). A rare intercomparison of nutrient analysis at sea: lessons learned and recommendations to enhance comparability of open-ocean nutrient data. *Earth System Science Data, 11*(1), 355-374. doi:10.5194/essd-11-355-2019

Meire, L., Mortensen, J., Meire, P., Juul-Pedersen, T., Sejr, M. K., Rysgaard, S., et al. (2017). Marine-terminating glaciers sustain high productivity in Greenland fjords. *Glob Chang Biol, 23*(12), 5344-5357. doi:10.1111/gcb.13801

Meire, L., Søgaard, D. H., Mortensen, J., Meysman, F. J. R., Soetaert, K., Arendt, K. E., et al. (2015). Glacial meltwater and primary production are drivers of strong CO₂ uptake in fjord and coastal waters adjacent to the Greenland Ice Sheet. *Biogeosciences, 12*(8), 2347-2363. doi:10.5194/bg-12-2347-2015

Melling, H., Agnew, T. A., Falkner, K. K., Greenberg, D. A., Lee, C. M., Münchow, A., et al. (2008). Fresh-Water Fluxes via Pacific and Arctic Outflows Across the Canadian Polar Shelf. In R. R. Dickson, J. Meincke, & P. Rhines (Eds.), *Arctic–Subarctic Ocean Fluxes: Defining the Role of the Northern Seas in Climate* (pp. 193-247). Dordrecht: Springer Netherlands.

Michel, C., Ingram, R. G., & Harris, L. R. (2006). Variability in oceanographic and ecological processes in the Canadian Arctic Archipelago. *Progress in Oceanography, 71*(2-4), 379-401. doi:10.1016/j.pocean.2006.09.006

Noble, A. E., Ohnemus, D. C., Hawco, N. J., Lam, P. J., & Saito, M. A. (2017). Coastal sources, sinks and strong organic complexation of dissolved cobalt within the US North Atlantic GEOTRACES transect GA03. *Biogeosciences, 14*(11), 2715-2739. doi:10.5194/bg-14-2715-2017

Oliver, H., Castelao, R. M., Wang, C., & Yager, P. L. (2020). Meltwater-Enhanced Nutrient Export From Greenland's Glacial Fjords: A Sensitivity Analysis. *Journal of Geophysical Research: Oceans, 125*(7). doi:10.1029/2020jc016185

Paden, J., J. Li, C. Leuschen, F. Rodriguez-Morales, and R. Hale (Producer). (2010, updated 2019). IceBridge MCoRDS L2 Ice Thickness, Version 1.

Raiswell, R., Hawkings, J., Elsenousy, A., Death, R., Tranter, M., & Wadham, J. (2018). Iron in Glacial Systems: Speciation, Reactivity, Freezing Behavior, and Alteration During Transport. *Frontiers in Earth Science, 6*. doi:10.3389/feart.2018.00222

Randelhoff, A., Holding, J., Janout, M., Sejr, M. K., Babin, M., Tremblay, J.-É., & Alkire, M. B. (2020). Pan-Arctic Ocean Primary Production Constrained by Turbulent Nitrate Fluxes. *Frontiers in Marine Science, 7*. doi:10.3389/fmars.2020.00150

RGI Constortium (2017). Randolph Glacier Inventory – A Dataset of Global Glacier Outlines: Version 6.0: Technical Report. *Global Land Ice Measurements from Space*, Colorado, USA. Digital Media. doi:https://doi.org/10.7265/N5-RGI-60

Schroth, A. W., Crusius, J., Hoyer, I., & Campbell, R. (2014). Estuarine removal of glacial iron and implications for iron fluxes to the ocean. *Geophysical Research Letters, 41*(11), 3951-3958. doi:https://doi.org/10.1002/2014GL060199

Seifert, M., Hoppema, M., Burau, C., Elmer, C., Friedrichs, A., Geuer, J. K., et al. (2019). Influence of Glacial Meltwater on Summer Biogeochemical Cycles in Scoresby Sund, East Greenland. *Frontiers in Marine Science, 6*. doi:10.3389/fmars.2019.00412

Straneo, F., & Cenedese, C. (2015). The Dynamics of Greenland's Glacial Fjords and Their Role in Climate. *Ann Rev Mar Sci, 7*, 89-112. doi:10.1146/annurev-marine-010213-135133

Tonnard, M., Planquette, H., Bowie, A. R., van der Merwe, P., Gallinari, M., Desprez de Gésincourt, F., et al. (2020). Dissolved iron in the North Atlantic Ocean and Labrador Sea along the GEOVIDE section (GEOTRACES section GA01). *Biogeosciences, 17*(4), 917-943. doi:10.5194/bg-17-917-2020

USGS (Producer). (2019). Landsat 8. Sioux Falls, South Dakota, USA. *Remote-sensing imagery*.

Van Wychen, W., Burgess, D. O., Gray, L., Copland, L., Sharp, M., Dowdeswell, J. A., & Benham, T. J. (2014). Glacier velocities and dynamic ice discharge from the Queen Elizabeth Islands, Nunavut, Canada. *Geophysical Research Letters, 41*(2), 484-490. doi:10.1002/2013gl058558

Van Wychen, W., Copland, L., & Burgess, D. (2020). Ice Masses of the Eastern Canadian Arctic Archipelago. In *Landscapes and Landforms of Eastern Canada* (pp. 297-314).

Van Wychen, W., Copland, L., Burgess, D. O., Gray, L., Schaffer, N., & Fisher, T. (2015). Glacier velocities and dynamic discharge from the ice masses of Baffin Island and Bylot Island, Nunavut, Canada. *Canadian Journal of Earth Sciences, 52*(11), 980-989. doi:10.1139/cjes-2015-0087

Van Wychen, W., Davis, J., Copland, L., Burgess, D. O., Gray, L., Sharp, M., et al. (2017). Variability in ice motion and dynamic discharge from Devon Ice Cap, Nunavut, Canada. *Journal of Glaciology, 63*(239), 436-449. doi:10.1017/jog.2017.2

Vibe, C. (1939). Preliminary investigations on shallow water animal communities in the Upernavik- and Thule-districts (N. W. Greenland). *Medd. om Gronl. , 124*(2), 42.

Wadham, J. L., Hawkings, J. R., Tarasov, L., Gregoire, L. J., Spencer, R. G. M., Gutjahr, M., et al. (2019). Ice sheets matter for the global carbon cycle. *Nat Commun, 10*(1), 3567. doi:10.1038/s41467-019-11394-4

Wehrmann, L. M., Formolo, M. J., Owens, J. D., Raiswell, R., Ferdelman, T. G., Riedinger, N., & Lyons, T. W. (2014). Iron and manganese speciation and cycling in glacially influenced high-latitude fjord sediments (West Spitsbergen, Svalbard): Evidence for a benthic recycling-transport mechanism. *Geochimica et Cosmochimica Acta, 141*, 628-655. doi:10.1016/j.gca.2014.06.007

Williams, P. L., Burgess, D., Waterman, S. N., Roberts, M., Bertrand, E. M., & Bhatia, M. (submitted). Nutrient and Carbon Export from a Tidewater Glacier to the Coastal Ocean in the Canadian Arctic Archipelago. *Journal of Geophysical Research - Biogeosciences*.

Wychen, W. V., Burgess, D., Kochtitzky, W., Nikolic, N., Copland, L., & Gray, L. (2021). RADARSAT-2 Derived Glacier Velocities and Dynamic Discharge Estimates for the Canadian High Arctic: 2015–2020. *Canadian Journal of Remote Sensing*, 1-23. doi:10.1080/07038992.2020.1859359

Zhang, R., John, S. G., Zhang, J., Ren, J., Wu, Y., Zhu, Z., et al. (2015). Transport and reaction of iron and iron stable isotopes in glacial meltwaters on Svalbard near Kongsfjorden: From rivers to estuary to ocean. *Earth and Planetary Science Letters, 424*, 201-211. doi:10.1016/j.epsl.2015.05.031

Zhang, Y., Chen, C., Beardsley, R. C., Gao, G., Lai, Z., Curry, B., et al. (2016). Studies of the Canadian Arctic Archipelago water transport and its relationship to basin-local forcings: Results from AO-FVCOM. *Journal of Geophysical Research: Oceans, 121*(6), 4392-4415. doi:10.1002/2016jc011634